International Journal of Biological Macromolecules 323 (2025) 147108

Contents lists available at ScienceDirect

International Journal of Biological Macromolecules

journal homepage: www.elsevier.com/locate/ijbiomac

Crystal structure and ligand binding of a sigma-class glutathione S-transferase associated with cross-resistance in a specialist herbivore

Timothy W. Moural [a,*], Jonathan A. Hernandez [a], Qi-Ren Chen [a], Sonu Koirala BK [a], Yanjun Liu [a], Tristan M. Cofer [a], Isadora X. Zuo [a,b], Andrei Alyokhin [c], Haichuan Wang [d], Fang Zhu [a,e,**]

[a] Department of Entomology, Pennsylvania State University, University Park, PA 16802, USA
[b] State College Area High School, State College, PA 16801, USA
[c] School of Biology and Ecology, University of Maine, Orono, ME 04469, USA
[d] USDA-ARS Agroecosystem Management Research Unit, Lincoln, NE 68583, USA
[e] Huck Institutes of the Life Sciences, Pennsylvania State University, University Park, PA 16802, USA

ARTICLE INFO

Keywords:
Insecticide resistance
Xenobiotic adaptation
Conjugation
X-ray crystallography
Molecular docking

ABSTRACT

Understanding the molecular mechanisms underlying insect adaptation is critical for elucidating the evolution of pesticide resistance and improving pest management strategies. While host plant preadaptation has been proposed to facilitate insecticide resistance, direct evidence remains limited. Here, we investigated a sigma-class glutathione S-transferase (GST), *LdGSTs2*, in the Colorado potato beetle (*Leptinotarsa decemlineata*), a major agricultural pest. *LdGSTs2* is significantly overexpressed in an imidacloprid-resistant strain and induced by host plant allelochemicals. Silencing *LdGSTs2* via RNA interference increased susceptibility to imidacloprid, supporting its functional role in resistance. Ligand-binding assays using 8-anilinonaphthalene-1-sulfonic acid (ANS) revealed that LdGSTs2 interacts with a broad range of insecticides and potato-derived phytochemicals. We further solved the 3D crystal structure of LdGSTs2 and performed molecular docking, which identified key residues involved in ligand interactions. These findings demonstrate that LdGSTs2 may contribute to cross-resistance by binding both synthetic and natural xenobiotics, without direct evidence of metabolic detoxification. Our results provide new mechanistic insights into how sigma-class GSTs facilitate adaptation to environmental toxins and highlight a potential molecular link between host plant use and insecticide resistance in specialist herbivores.

1. Introduction

The Colorado potato beetle (CPB), *Leptinotarsa decemlineata*, is a global agriculture pest of the potato, *Solanum tuberosum*, and other Solanaceae crops (e.g. tomato, eggplant). This insect causes significant damage to potato crops by defoliation, which results in millions of dollars of crop loss [1,2]. Over the past several decades, chemical control using various insecticides has remained the cornerstone of CPB management. However, this approach has led to widespread insecticide resistance in beetle populations. Since the middle of last century, CPB has developed resistance to more than 50 different active ingredients, including all major insecticide classes. Laboratory selection also produced a strain resistant to a recently developed double-stranded RNA (dsRNA)-based insecticidal compound [2–6]. As a specialist herbivore, CPB mainly feeds on Solanaceae family plants which are enriched in diverse plant secondary metabolites such as phenolic acids, glycoalkaloids, flavonoids, and their derivatives in flowers, leaves, stems and other tissues [7]. These secondary metabolites do not directly participate in plant growth or development, but play crucial roles in defending plants against bacteria, fungi, viruses, and insect herbivores, thereby enhancing plant fitness under stress conditions [8]. For instance, phenolic acids are among the major phenolic compounds in potato plants and are characterized by one or more hydroxyl groups attached to an aromatic ring [8,9]. These compounds can be directly toxic to herbivores or enzymatically oxidized by peroxidases or polyphenol oxidases into reactive quinones and other toxic metabolites that impair insect

* Corresponding author.
** Correspondence to: F. Zhu, Huck Institutes of the Life Sciences, Pennsylvania State University, University Park, PA 16802, USA.
E-mail addresses: twm78@psu.edu (T.W. Moural), fuz59@psu.edu (F. Zhu).

https://doi.org/10.1016/j.ijbiomac.2025.147108
Received 27 July 2025; Received in revised form 15 August 2025; Accepted 23 August 2025
Available online 25 August 2025

growth and development [8,10–12]. Other secondary metabolites found in potato, such as caffeic acid, α-solanine, and α-chaconine, also serve as plant defense compounds and negatively impact the development, growth, and biochemical physiology of insects [13–15].

It has been proposed that the long evolutionary history of coping with toxic secondary metabolites in host plants has likely contributed to the Colorado potato beetle's robust ability to develop insecticide resistance [16,17]. This adaptation is thought to be mediated, at least in part, by shared metabolic detoxification pathways [18]. Specifically, metabolic detoxification involving cytochrome P450s, glutathione S-transferases (GSTs), uridine diphosphate-glycosyltransferases (UGTs), and carboxylesterases is considered to be one of the most dominant cross-resistance mechanisms potentially linking adaptation to host plant toxins with the development of insecticide resistance [17–23]. Among these enzymes, GSTs consist of a large family of multifunctional enzymes distributed throughout various organisms (e.g. animals, plants, arthropods) [24]. GSTs are involved in Phase II of the xenobiotic detoxification process and also have other functions such as in oxidative stress and hormone transport [25]. GSTs function by catalyzing the conjugation reaction of electrophilic compounds with the thiol group of reduced glutathione (GSH), resulting in products that are more water-soluble and excretable than the uncatalyzed substrates [26]. In addition, GSTs, as part of the antioxidant enzyme system, help protect against oxidative stress induced by pesticides, plant allelochemicals, and various other abiotic stressors [27,28]. This versatility enables GSTs to act on a broad spectrum of substrates, facilitating adaptation to both host plant defenses and synthetic insecticides [21,25].

GSTs can be classified into three categories based on cellular location: cytosolic, microsomal, or mitochondrial GSTs. However, only cytosolic and microsomal GSTs have been discovered in insects [21,29]. Cytosolic GSTs are water soluble enzymes and can be further classified into six classes: zeta, theta, sigma, omega, delta, and epsilon – based on sequence, structure and function, with delta and epsilon classes being specific to insects [30,31]. Sigma class of GSTs comprises one of the largest classes identified across both vertebrates and invertebrates [32]. It is believed to have evolved from ancestral GST genes and exhibits enzymatic activity toward the common substrates 1-chloro-2,4-dinitrobenzene (CDNB), 4-hydroxynonenal (HNE) which is a lipid peroxidation (LPO) product [29,33]. Sigma class GSTs have been implicated in both insecticide resistance and adaptation to host plant defenses, primarily through their roles in mitigating oxidative stress [33]. For example, *NlGSTs1* and *NlGSTs2* have been shown to contribute to insecticide resistance in the brown planthopper, *Nilaparvata lugens,* partly due to their antioxidant functions. These same mechanisms also appear to help protect *N. lugens* against rice plant defense [34]. The number of GST genes in a genome varies across insect species from 41 in the red flour beetle, *Tribolium castaneum*, to 11 in *N. lugens*. Previous studies have shown that GSTs contribute resistance against various insecticides in several CPB populations [35–38]. Recent genome and transcriptome analyses have identified 30 *LdGST*s, including 4 sigma, 3 delta, 10 epsilon, 5 theta, and 1 zeta GSTs [21,39]. While one functional characterization study [40] and one RNAi-based investigation have begun to explore the roles of specific GSTs in CPB [38], the broader functional significance of these genes in xenobiotic adaptation remains largely uncharacterized.

In this study, we investigated the functional role of a novel GST gene, *LdGSTs2*, identified in the CPB [39–41]. *LdGSTs2* was significantly overexpressed in the resistant CPB strain compared to the susceptible one, and its expression was further induced upon feeding on potato leaves. Based on these findings, we hypothesized that *LdGSTs2* facilitates its robust capability toward insecticide resistance and host plant adaptation. To test our hypothesis, we silenced *LdGSTs2* by RNAi and evaluated its effect on susceptibility of the CPB to imidacloprid. We further expressed recombinant LdGSTs2 protein in *E. coli* to characterize its kinetic parameters and substrate specificity. Finally, we determined the X-ray crystal structure of LdGSTs2 and conducted protein-ligand interaction analysis using the crystal structure and molecular docking to gain structural perceptions into substrate recognition. Together, our findings provide mechanistic insights into how a GST like *LdGSTs2* may mediate cross-resistance to both plant toxins and insecticides, shedding light on the molecular basis of the remarkable adaptive capacity in this notorious agricultural pest.

2. Materials and methods

2.1. Insects

A laboratory-maintained susceptible colony of *Leptinotarsa decemlineata* was originally acquired from French Ag Research, Inc. (Lamberton, MN) and has since been propagated without any pesticide exposure [40]. The insecticide-resistant population used in this study was collected from the University of Maine's Aroostook Research Farm (Presque Isle, ME, USA) [42]. Both colonies were maintained on *Solanum tuberosum* cv. Red Norland in separate BugDorm insect rearing cages (MegaView Science Co., Ltd.) maintained in a greenhouse facility at Penn State, under controlled conditions (25 ± 5 °C, 16, 8 h light, dark cycle). Pesticide-free potato plants were supplied weekly to ensure continuous food availability. Eggs were collected daily and incubated in petri dishes under consistent environmental conditions (25 ± 1 °C, 70 % relative humidity, 16, 8 h L, D). Upon hatching, larvae were fed fresh potato foliage until reaching the second instar, at which point they were returned to the greenhouse cages with whole plants for continued development.

2.2. Bioinformatics & phylogenetic analysis

LdGSTs2 was identified from our previous transcriptomic study of CPB and exhibited 100 % sequence similarity to XP_023025843.1 from the CPB [16,40]. A total of 149 GST amino acid sequences from four different insect species, *Drosophila melanogaster*, *Apis mellifera*, *Tribolium castaneum*, and *L. decemlineata* were retrieved from NCBI database (https://www.ncbi.nlm. nih.gov) (Table S1). Multiple sequence alignment was performed using MUSCLE in MEGA11 at default settings. Maximum likelihood (ML) unrooted phylogenetic tree was then inferred using RaxML 8.2.12 [43–45]. Confidence on each phylogenetic tree was assessed with 500 bootstrap replications. Additionally, the isoelectric point, molecular weight, and extinction coefficient were calculated using Expasy ProtParam tool (https://web. expasy.org/protparam/), and a signal peptide analysis was conducted with Signal 4.1 server (http://www.cbs.dtu.dk/services/SignalP-4.1/).

2.3. RNA extraction & cDNA synthesis

Total RNA was prepared from three replicates of pooled samples, including eight developmental stages and six body parts/organs from both susceptible and resistant CPB populations. For developmental stages, a set number of samples was collected for each replicate: 1-day egg (50 eggs), 5-day egg (50 eggs), 1st instar larva (10 individuals), 2nd instar larva (10 individuals), 3rd instar larva (five individuals), 4th instar larva (three individuals), pupa (three individuals), adult male (three individuals) and adult female (three individuals). Six different samples were collected from 5 to 15 females (1-week old) per replicate from both susceptible and resistance strains, including head, leg, midgut, fat body, ovary, and Malpighian tubules. Three independent replicates were performed. Trizol Reagent (Invitrogen) was used to extract RNA for each pooled sample by following the manufacturer's protocol. Extracted RNA was then treated with Invitrogen Turbo™ DNAse (Thermo Fisher Scientific, Waltham, MA, USA) to eliminate genomic DNA contaminant. The RNA quality and quantity were evaluated with a NanoDrop One Microvolume UV–Vis Spectrophotometer (Thermo Scientific, Madison, WI, USA). The A260/280 value of 1.8–2.0 was used as a standard to assess RNA quality. 5 μg purified RNA samples

were then used for cDNA synthesis with M-MLV reverse transcriptase kit (Promega, Madison, WI, USA) following the manufacturer's protocol.

2.4. Induction assays

To test the role of *LdGSTs2* in the induction of plant allelochemicals, two treatments of potato leaves and artificial diet (Colorado potato beetle diet, Bio-Serv, Frenchtown, NJ) were used. The resistant beetles were starved for 24 h and then fed either 0.5 g of fresh potato leaves or artificial diet. The control insects were fed on an artificial diet for 48 h. The plant allelochemical treated beetles were fed on artificial food for 24 h and then fed on potato leaves for 24 h as described in our previous study [16]. The midgut samples without gut contents were then collected for RNA extraction and cDNA synthesis as described previously. Three replicates with five adult CPB females per replicate were used for this induction assay.

2.5. Quantitative real-time PCR (qRT-PCR)

qRT-PCR was performed in a CFX96 Touch real-time PCR detection system (Bio-Rad Laboratories, Hercules, CA) for the expression of *LdGSTs2* in samples following the procedure described in our previous study [40]. Each reaction consisted of 5.0 μL SsoAdvanced™ Universal SYBR Green Supermix (Bio-Rad Laboratories, Hercules, CA), 1.0 μL cDNA, 3.6 μL ddH_2O, and 0.4 μL of forward and reverse primers (Table S2). An initial incubation of 95 °C for 3 min, followed by 35 cycles of 95 °C for 10 s, 55 °C for 30 s, 95 °C for 10 s, and 65 °C for 5 s settings were used. Two reference genes, elongation factor 1α (*Ef1α*) and ribosomal protein L4 (*Rpl4*) were used for relative expression of *LdGSTs2* with the $2^{-\Delta\Delta CT}$ method [16,46,47]. Primers with efficiency (95 % < E < 105 %) at $R^2 > 0.99$ were used in qRT-PCR. Three biological replicates and three technical replicates were conducted.

2.6. RNA interference and bioassay

The dsRNAs were synthesized using the MEGAscript RNAi kit (Invitrogen) with primers tailed with T7-TAATACGACTCACTATAGGG (Table S2) by following manufacturer's instruction. A pET His6 GFP TEV LIC cloning vector plasmid (addgene#29663) was used as template for a green fluorescent protein (GFP) gene (ds*GFP*) dsRNA synthesis. The dsRNA was then purified using an Invitrogen Turbo DNA-*free*™ Kit (Thermo Fisher Scientific, Waltham, MA, USA) by following protocol with kit. The concentration of dsRNA was measured using NanoDrop One (ThermoFisher). The dsRNA feeding bioassay was performed as in our previous studies [46,48]. In brief, 1-week old female beetles showing normal activity and no visible abnormalities were starved for 24 h before initiation of the bioassay. Each replicate consisted of 10 female individuals with additional individuals reserved for assessing knockdown efficiency. Each replicate also included a corresponding control group. Two female beetles were provided with a leaf disc (2 cm in diameter) that had 10 μg ds*LdGSTs2* or ds*GFP* (5 μg/beetle) dissolved in 30 μL of ddH_2O in a 6 cm diameter petri dish. Each beetle was fed 5 μg dsRNA daily for two consistent days, followed by one day of feeding on fresh potato leaves only. The beetles then were submitted to knockdown efficiency assessment or bioassay. For knockdown efficiency assessment, total RNA was extracted from beetles in each replicate and used to synthesize cDNA for qRT-PCR. Six biological replicates were conducted independently. The relative expression of *LdGSTs2* in female beetles fed ds*LdGSTs2* or ds*GFP* was calculated and compared.

For the bioassay, 10 female beetles fed ds*LdGSTs2* or ds*GFP* were anesthetized for 15 min on ice prior to the assay. 1 μL (1 μg/μL) imidacloprid (99.5 % purity, Sigma Aldrich, St. Louis, MO, USA) dissolved in acetone was applied to the ventral surface of the penultimate abdominal segment using a Hamilton 25 μL model #702 syringe (Hamilton, Reno, NV, USA). The control beetles were treated with the same volume of acetone only. After treatment, all CPBs were kept on ice for about 10 min and then transferred to fresh petri dishes containing potato leaves and maintained in a rearing room at 25 ± 1 °C, 60 % ± 5 %, and a 16:8 photoperiod regime. CPB mortality was assessed at 24- and 48-h post-treatment. The determination of mortality in an individual CPB to pesticide treatment was adapted from prior studies [49,50] using three criteria [51]. Six biological replicates were conducted independently for control and treatment.

2.7. Heterologous expression and purification

A construct with the codon optimized *LdGSTs2* coding region and a C-terminal his-tag (QVLEHHHHHH) cloned into a pET30a plasmid (GenScript®). The plasmid then was transformed into Rosetta™ II (DE3) pLysS cells and grown on lysogeny broth (LB) agar plates, transformants were selected for with antibiotics (50 μg/mL kanamycin and 25 μg/mL chloramphenicol). Five colonies were selected and confirmed with PCR for *LdGSTs2* insert. Positive colonies were grown up in 5 mL of LB supplemented with antibiotics in shaking incubator at 37 °C overnight (Thermo Scientific MaxQ 6000 Incubated Stackable Floor Shaker). Stock cells cultures were centrifuged overnight at 3000 rpm (Thermo Sorvall Legend XTR refrigerated centrifuge) at 4 °C and pellets were resuspended in 70 % LB:30 % glycerol and stored at −80 °C for use as stock cultures.

For expression of the LdGSTs2 protein, overnight 50 mL cultures started from stock culture stabs were grown at 37 °C in terrific broth (TB) with antibiotics (50 μg/mL kanamycin and 25 μg/mL chloramphenicol) and then used to inoculate a 1.2 L TB culture in a Fernbach shake flask, incubated at 37 °C and at 250 rpm in a shaking incubator (Thermo Scientific MaxQ 6000 Incubated Stackable Floor Shaker) until OD_{600nm} reached 0.8. The culture was then cooled in an ice bath and induced by adding isopropyl β-d-1-thiogalactopyranoside (IPTG) to a concentration of 0.5 mM, followed by further incubation at 20 °C and at 250 rpm shaking for an additional 21 h. Cells were harvested by centrifugation at 3500 rpm (Thermo Sorvall Legend XTR refrigerated centrifuge) for 15 mins at 4 °C and the cell pellets were frozen at −20 °C until needed for purification.

For purification of LdGSTs2, cell pellets were resuspended in five volumes of lysis buffer (per pellet volume) at pH 7.2 containing 50 mM NaPi, 500 mM NaCl, 20 mM Imidazole, and one EDTA-free protease inhibitor tablet (Thermo Scientific™ Pierce™) per 50 mL. Cells were lysed on ice by sonication using a Branson Digital Sonifier SFX 150 at 70 % amplitude for 30 s per pulse, repeated 5–7 times. Then, soluble proteins were separated from insoluble debris by centrifugation at 18,000 ×*g*. The resulting supernatant was applied to a Ni-NTA affinity column pre-equilibrated with binding buffer (50 mM NaPi, 300 mM NaCl, 20 mM imidazole, pH 7.2). The column was then washed with the same buffer to remove nonspecifically bound proteins. LdGSTs2 was eluted using an elution buffer containing 50 mM sodium phosphate, 300 mM NaCl, and 250 mM imidazole (pH 7.2). Using an NGC Medium-Pressure Liquid Chromatography System (Bio-Rad®), the purified protein was subjected to a 100× buffer exchange into 20 mM MES, 5 mM DTT (pH 6.5), and applied to a HiScreen Capto SP ImpRes column (Cytiva®). A linear gradient of over 20 column volumes (CV) from buffer A (20 mM MES, 5 mM DTT, pH 6.5) to buffer B (20 mM MES, 5 mM DTT, 1 M NaCl, pH 6.5) was run to wash and elute LdGSTs2. SDS-PAGE was performed to analyze the fractions containing LdGSTs2. These fractions were then pooled and concentrated to 1 mL, followed by injection onto a HiLoad Superdex 200 pg size exclusion column (Cytiva®) connected to an NGC Medium-Pressure Liquid Chromatography System (Bio-Rad®), and eluted with flow rate of 0.5 mL/min, using a buffer of 20 mM MES, 150 mM NaCl, 5 mM DTT, and 1 mM EDTA at pH 6.5. Elution was concentrated to 30 mg/mL and flash frozen with liquid nitrogen and stored at −80 °C for later use. Purified LdGSTs2 concertation was calculated using the extinction coefficient $\lambda_{280nm} = 1.045\ L{\cdot}g^{-1}{\cdot}cm^{-1}$.

2.8. LdGSTs2 glutathione conjugation activity

Enzyme assays for recombinant LdGSTs2 were performed at a reaction volume of 200 μL in 96-well UV-star® (Greiner Bio-One) microplates, using a Spark® multi-mode plate reader (TECAN) set at 30 °C. Path-length corrected molar attenuation coefficients were used for calculations. Controls without enzyme were run to account for non-catalytic enzyme reaction contributions and all assays were run in triplicate. A pH activity profile was conducted across a range of pH 6.0 to pH 8.0 using 100 mM potassium phosphate buffer. The pH assay was performed by changing the ratio of KH_2PO_4 to K_2HPO_4 to maintain precise pH control throughout the assay. CDNB and GSH were each held at concentration of 1 mM and LdGSTs2 was at 0.05 mg/mL, wavelength was read at 340 nm every 10 s for 1 min and 10 s. Enzyme kinetics parameters were determined using model substrate CDNB and GSH with a method modified from Habeg et al. 1974 [26]. The assay buffer contains 100 mM potassium phosphate with pH at 7.2. For the CDNB assay, GSH was held constant at 4 mM and CDNB varied from 0.25 mM to 6 mM with LdGSTs2 at 0.1 mg/mL. For the GSH, CDNB was held constant at 2 mM and GSH varied from 0.0625 mM to 8 mM. The GSH kinetic parameters were calculated by fitting data to Michaelis-Menten plot with non-linear regression in GraphPad Prism 10.4.1. For the variable concertation CDNB assay, the plot displayed a sigmoidal character. Therefore, model comparison was performed using Akaike's Information Criterion (AIC) to evaluate the fit of the Michaelis-Menton model verses an allosteric sigmoidal model.

2.9. Fluorescence binding assay

Competitive fluorescence binding assay was performed by using ANS as a fluorescent probe to investigate the capability of various ligands to bind the H-site of LdGSTs2. ANS has been used in previous studies to investigate ligands that bind to hydrophobic pockets in proteins. In the case of GSTs, ANS has been shown to bind at a 1:1 molar ratio [52–54]. For LdGSTs2, a saturation binding assay with ANS was performed in assay buffer 100 mM KPi, pH 6.5, with LdGSTs2 concertation held at 2 μM, and ANS concentration varied from 0 μM to 128 μM. The K_d for ANS was found by fitting a hyperbolic binding curve in GraphPad Prism 10.4.1, with non-linear regression using fitting equations developed by Richard Neubig [55,56]. For ligand competition assay, LdGSTs2 was held at 2 μM, ANS at 25 μM, and ligands were varied from 15.625 μM to 2.0 mM. Assays were run in a total volume of 200 μL per reaction in black flat bottom 96-well plates, incubated for 10 mins at 30 °C, and fluorescence intensity was measured in a Tecan Spark® plate reader with 380 nm/20 nm excitation filter and 485 nm/20 nm emission filter. Known ligands to commonly bind GST H-sites, including CDNB, *p*-nitrophenyl acetate (PNA), and ethacrynic acid (EA) were used as assay positive controls. GSH was used as a negative control as it binds to the G-site. Ligands tested included the insecticides acephate, carbaryl, chlorpyrifos, malathion, methamidophos, acetamiprid, clothianidin, imidacloprid, and thiamethoxam; the herbicides 2,4-D, dicamba, fenoprop, picloram, and triclopyr; the fungicide propiconazole; the natural products caffeic acid, cinnamaldehyde, chlorogenic acid, p-coumaric acid, and vanillin; and the pesticide metabolites 6-chloronicotinic acid, 2,4-dichlorophenol, and 3,5,6-trichloro-2-pyridinol (TCPy). Fluorescence inhibition curves were generated in GraphPad Prism 10.4.1 to calculate IC50 values for competitive ligands, which were then used to calculate dissociation constants (K_i) with the equation $K_i = (IC50)/(1 + [ANS]/K_d\text{-ANS})$ [57]. The assays were run in triplicate.

2.10. Protein crystallization and molecular docking

LdGSTs2 crystallization was conducted by using sitting drop vapor diffusion method at 20 °C as described in our previous study [40]. LdGSTs2 was added to sitting drop well at a concentration of 15 mg/mL and mixed with a reservoir solution (100 mM Tris with pH at 8.5, 0.1 mM $MgCl_2$, and 30 % *w/v* PEG 3350) in a 1:1 ratio, followed by incubation at 20 °C. Crystal growth was assessed daily over a prolonged period. Due to the poor diffraction quality of the initial crystals, microseeding was explored to facilitate the growth of higher-quality crystals. The resulting crystals were cryoprotected in mother liquor containing 37.5 % w/v glucose. Cryoprotected crystals were flash frozen in liquid nitrogen (LN2) and shipped to Macromolecular X-ray science at the Cornell High Energy Synchrotron Source (MacCHESS) beamline 7B2 for remote data collection. The XDS software package, CCP4 software suite and AIMLESS were used for data processing, initial phasing was done with molecular replacement using PBD ID 5H5L and Phenix Phaser-MR program, initial model building was done with Phenix Autobuild, refinement was done using Phenix Refine, Coot, Phenix feature-enhanced map, and using an AlphaFold2 model for restraints [58–68]. Structural analysis was performed with UCSF Chimera, UCSF ChimeraX, PyMOL (http://www.pymol.org/pymol), CavitOmix pymol plugin with LIGSITE algorithm, the PISA program (Proteins, Interfaces, Structures and Assemblies) made available by the European Bioinformatics Institute at http://www.ebi.ac.uk/pdbe/prot_int/pistart.html, and Coot [61,69–72]. Structure figure images were rendered with UCSF ChimeraX [70]. For molecular docking, chlorogenic acid and chlorpyrifos were downloaded from PubChem (https://pubchem.ncbi.nlm.nih.gov), docking was done with AutoDock Vina via the DockingPie 1.2 plugin installed in PyMOL 3.0.4 with exhaustiveness set to 20, possible poses set to 10, and the grid box was set to cover the volume of the active site.

2.11. Statistical analysis

Data presented in this study were presented as standard means ± SE. A Student's *t*-test was used to analyze the differential expression profile of *LdGSTs2* between the two CPB populations. Significance was denoted as ** representing $p < 0.01$, *** for $p < 0.001$. One-way ANOVA with Tukey's test was used to analyze the developmental and spatial expression profiles of *LdGSTs2* among samples. Statistical significance among samples was denoted by distinct alphabetical letters (e.g. a, b, c), where identical letters next to the means denote no significant difference. SPSS 2.0 statistical software program (Chicago, IL) was used for analysis.

3. Results

3.1. Phylogenetic analysis

As illustrated in Fig. 1, the maximum likelihood phylogenetic analysis showed that LdGSTs2 is most closely related to the sigma GSTs from other well-studied insects, including *D. melanogaster*, *A. mellifera*, *T. castaneum*, and *L. decemlineata*. The highest similarity to other insect GSTs was observed with a sigma GST from *T. castaneum* (XP_008190960.1), showing an 44.12 % sequence identity at protein level. The accession numbers, species names, and GST classifications for all sequences used in constructing the phylogeny are listed in Table S1.

3.2. Expression profiles of LdGSTs2

The differential expression of *LdGSTs2* revealed a 2.8-fold increase of *LdGSTs2* expression in the resistant CPB strain compared to the susceptible strain (Fig. 2A). Among the six tissues tested, *LdGSTs2* showed the highest expression in both midgut and Malpighian tubules from both CPB strains. A significantly higher expression-1.9-fold difference was observed in the Malpighian tubules from the resistant strain compared to the susceptible one (Fig. 2B). In the potato leaf induction assay, *LdGSTs2* expression in the midgut of adult females reached 18-fold higher after 48 h of feeding on potato leaves compared to beetles fed on the artificial diet (Fig. 2C). In addition, across the development stages, the highest expression of *LdGSTs2* was observed in the adult female stage, while the

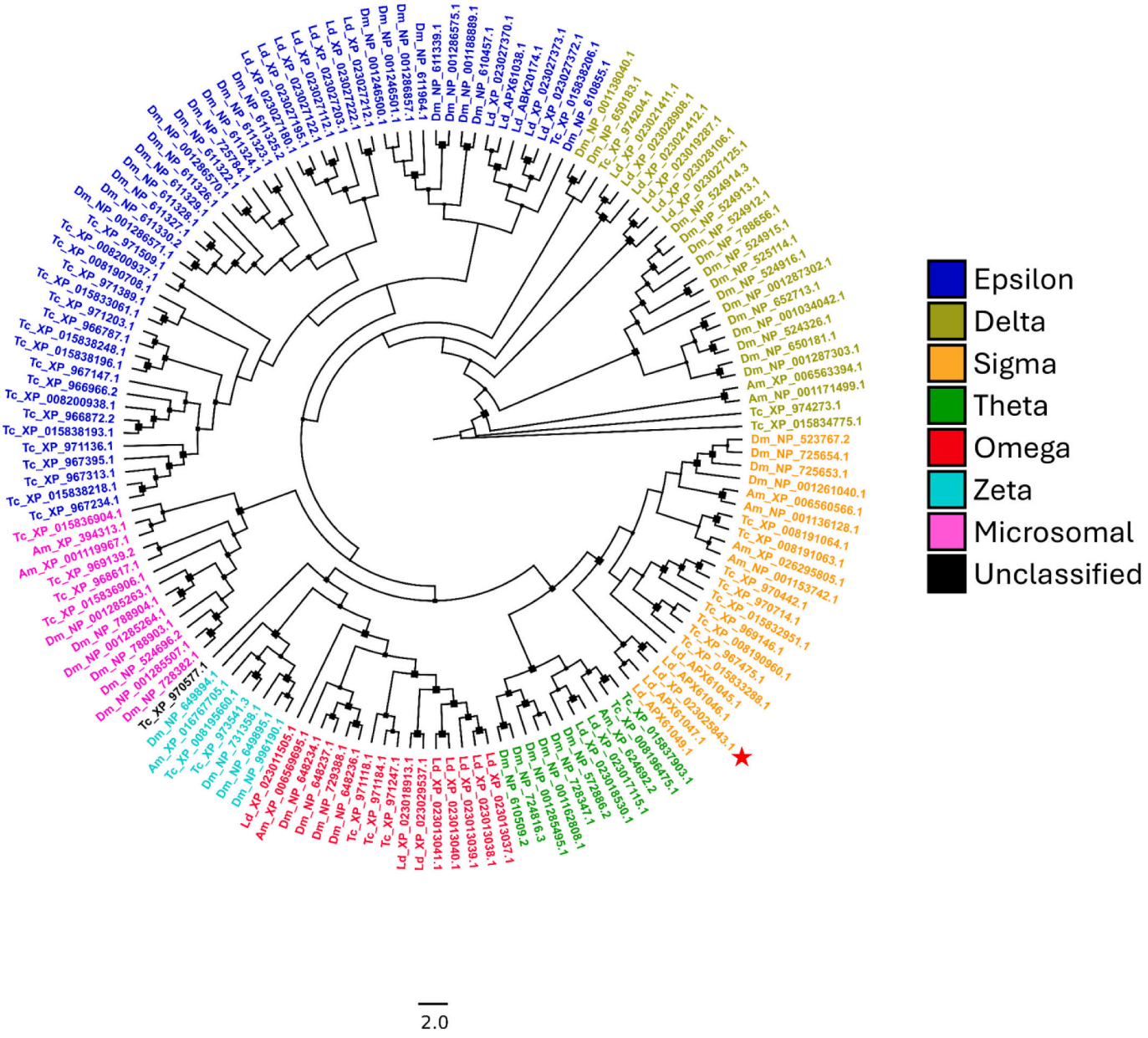

Fig. 1. Phylogeny Tree of LdGSTs2 with other GSTs from *Drosophila melanogaster*, *Bombyx mori*, *Manduca sexta*, *Tribolium castenum*, and *Anopheles gambiae*.

lowest expression occurred in the eggs (1-day and 5-day) and pupa stages (Fig. 2D) in both strains.

3.3. LdGSTs2 silencing enhanced insecticide susceptibility

To test whether *LdGSTs2* is involved in insecticide resistance, we examined the effect of *LdGSTs2* RNAi on insecticide susceptibility of female CPB adults. The mortality of 1-week old female CPB adults treated with 1 μg imidacloprid were examined and compared between ds*GFP* feeding beetles and ds*LdGSTs2* feeding beetles at 24- and 48-h post-treatment. As shown in Fig. 3A, following treatment, RNAi with ds*LdGSTs2* through feeding achieved a successful 90 % reduction in *LdGSTs2* expression. The silencing of the *LdGSTs2* did not lead to more mortality in 24-h post-treatment compared to the beetles fed ds*GFP*. However, after 48 h, beetles fed on ds*LdGSTs2* showed significantly higher mortality than that in the control (Fig. 3B).

3.4. LdGSTs2 kinetic parameters

LdGSTs2 was expressed recombinantly and purified to homogeneity using chromatographic methods detailed in materials and methods, final product was visualized using SDS-PAGE, and a single protein band was seen at ~25 kDA (Fig. S1). The molecular mass of the LdGSTs2 construct was calculated with Expasy Compute pI/Mw, to be 25.777 kDa, and pI to be 7.78. Based on the pH profile assay, using the model substrate CDNB, the highest GSH transferase activity toward CDNB tested was at pH 7.2 (Fig. S2). Since LdGSTs2 is a two-substrate enzyme, LdGSTs2 was also assayed with variable GSH concentration with constant CDNB concentration and with variable CDNB concentration and fixed GSH concentration. The resulting data, obtained using varied GSH concentration and fixed CDNB concentration, fit a typical hyperbolic curve and Michaelis-Menten kinetic parameters were calculated (Fig. 4 and Table 1). The V_{max}, K_m, k_{cat}, and k_{cat}/K_m values for GSH were 197.07 ± 5.35 μM/min, 0.13 ± 0.02 mM, 50.80 min^{-1}, 390.77 $min^{-1} \cdot mM^{-1}$, respectively. When CDNB concentration was varied and GSH

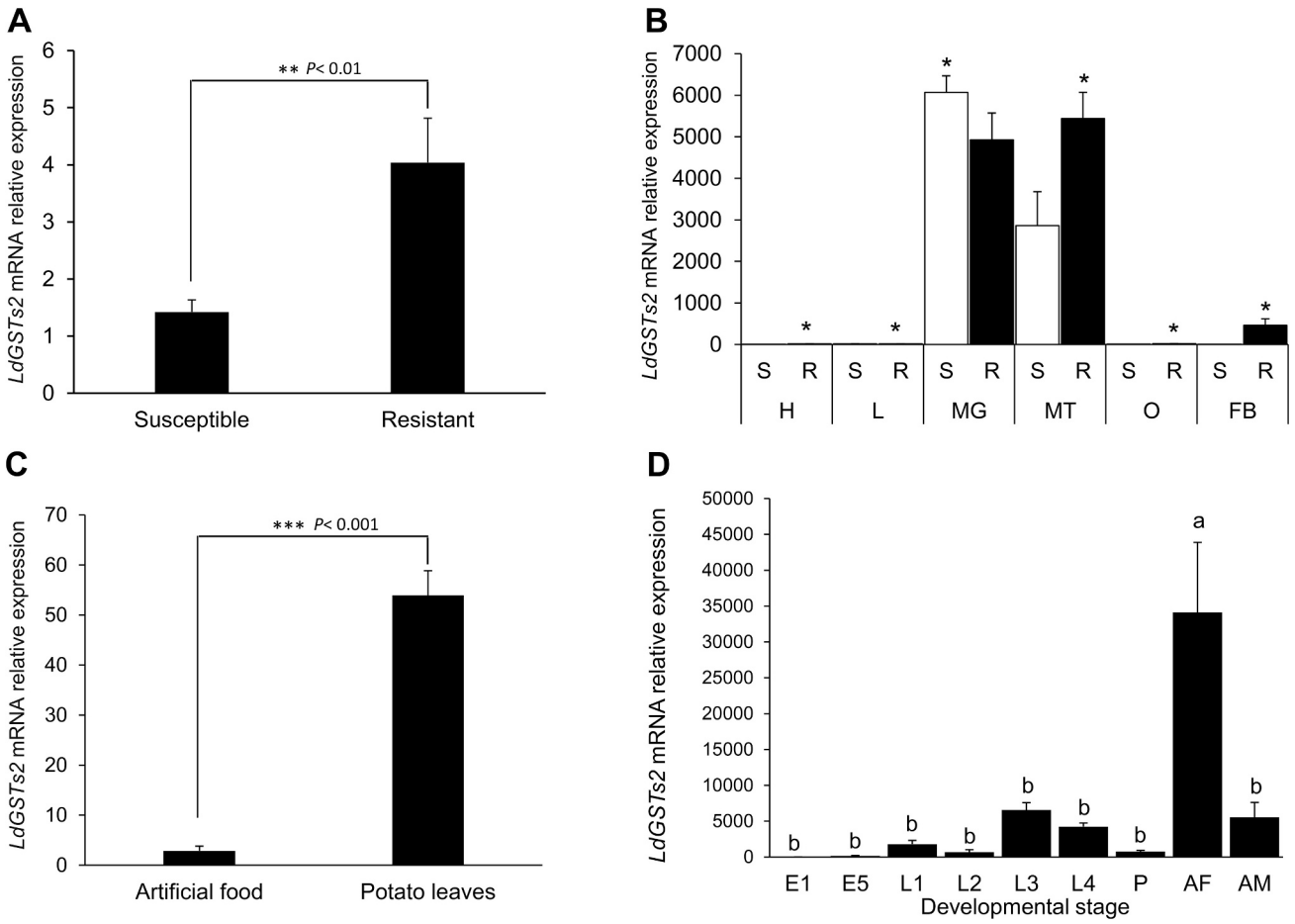

Fig. 2. mRNA expression patterns of *LdGSTs2*. (A) Differential expression between the susceptible and resistant CPB strains. (B) Expression profile of insect tissues in susceptible and resistant CPB strains. H represents head, L represents leg, MG represents midgut, MT represents Malpighian tubules, O represents ovary, and FB represents fat body. (C) Differential expression of *LdGSTs2* in the adult female beetles fed on artificial diet or potato leaves. (D) Expression profile of *LdGSTs2* in all CPB developmental stages of both susceptible and resistant strains. E1, E5 stand for 1-day and 5-day egg; L1–L4 represent 1^{st} – 4^{th} instar larvae; P represents pupa; AF stands for 1-week old adult female; and AM stands for 1-week old adult male. Student's *t*-test used for analysis between two samples. *P* value <0.05, 0.01, 0.001 are denoted as significant *, **, and ***, respectively, indicating statistical significance. One-way ANOVA followed by a Tukey's HSD test was used for analysis the difference among expressions in various developmental stages with SPSS 2.0 statistical analysis software. Different letters indicate a significant difference at $P < 0.05$.

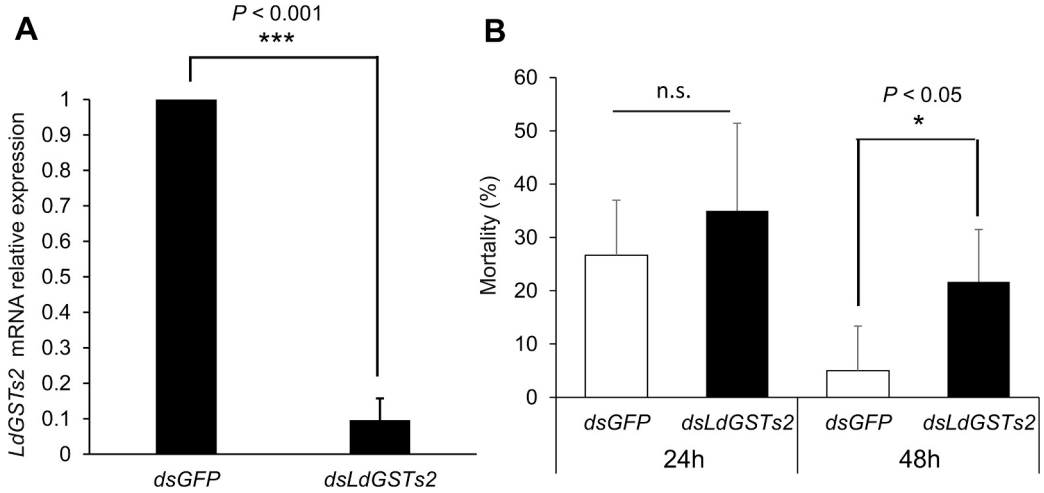

Fig. 3. Effect of *LdGSTs2* gene silencing on insecticide susceptibility of female CPB beetles. (A) The mRNA levels of *LdGSTs2* in whole body were quantified by qRT-PCR at the 4th day after the feeding dsRNA initiation. The relative mRNA levels were shown as a ratio in comparison with the levels of *Ef1α* and *Rpl4* mRNA. The data shown are mean + SEM ($n = 3$). (B) Mortalities of CPBs at 24 and 48 h after exposure to 1 μg imidacloprid/beetle (LD_{50}). The bioassay was performed 3 days after feeding ds*GFP* or ds*LdGSTs2*. Statistical significance of the gene expression or mortality between two samples was calculated using Student's *t*-test. ***$P < 0.001$, *$P < 0.05$.

concentration held fixed, the data plotted as a sigmoidal curve and was fit to the Hill equation. The resulting kinetic parameters were V_{max} = 1023.12 ± 73.64 μM/min, K_{half} = 3.20 ± 0.02 mM, k_{cat} = 263.73, k_{cat}/K_m = 82.41, and a Hill coefficient (h) of 1.54 ± 0.11.

3.5. LdGSTs2 binds to a broad range of pesticides and potato-derived phytochemicals

After confirming that LdGSTs2 could metabolize the model substrate CDNB *in vitro*, the ligand spectrum of LdGSTs2 was investigated with a competitive fluorescence binding assay using ANS as the fluorescence probe. Ligands from multiple chemical classes were screened, including model GST substrates, insecticides, herbicides, fungicide, pesticide metabolites, and natural products for their ability to displace ANS from LdGSTs2 and decrease fluorescence intensity.

First, for the competitive ligand fluorescence binding assay, the affinity of the fluorescent probe ANS was determined by fitting a nonlinear regression saturation binding curve (Fig. 5A). The resulting K_d of LdGSTs2 toward ANS was 25.20 ± 0.98 μM. Next, data obtained from the competitive fluorescence binding assay was used to plot inhibition curves (Fig. 5A) and fit respective IC50 values. For ligands that gave at least 50 % fluorescence inhibition, K_i values were calculated with the Cheng and Prusoff equation [73] and listed in Table 2.

Model substrates (CDNB, PNA, and EA) were tested to assess the appropriateness of the ANS competitive binding assay with LdGSTs2 (Fig. 5B). For the G-site substrate GSH, no IC50 value could be determined as the maximum inhibition of fluorescence only reached 21 %. These findings confirmed that the binding of GSH to LdGSTs2 had minimal impact on ANS binding, indicating that the experiment was effective and support the conclusion that GSH and ANS interact primarily with the G-site and H-site, respectively. For the model substrates that bind to the H-site- CDNB, EA, and PNA- exhibited greater than 50 % fluorescence inhibition, resulting in IC50 values of 1.199 ± 0.057 mM, 0.280 ± 0.005 mM, and 0.828 ± 0.093 mM, respectively. The calculated K_i values were 0.755 mM for CDNB, 1.123 mM for EA, and 0.262 mM for PNA (Table 2). In addition to model substrates, multiple insecticides from the organophosphate, carbamate, and neonicotinoid classes were tested (Fig. 6A). The only insecticide tested that was able to effectively displace ANS from the H-site and inhibit fluorescence was organophosphate chlorpyrifos (Fig. 6A), resulting in an IC50 of 0.166 ± 0.016 mM and K_i of 0.155 mM. Among additional pesticides tested (Fig. 6B) including multiple herbicides and the triazole fungicide propiconazole, only herbicides fenoprop and triclopyr reached 50 % or greater fluorescence inhibition (Fig. 6B). Titration of LdGSTs2:ANS with fenoprop resulted in an IC50 of 0.257 ± 0.003 mM and a K_i of 0.241 mM, while triclopyr had an IC50 of 1.572 ± 0.068 mM and K_i of 1.472 mM. In addition, multiple natural products and pesticide metabolites, such as caffeic acid, cinnamaldehyde, chlorogenic acid, vanillin, 2,4-dichlorphenol and TCPy, were also able to inhibit fluorescence by more than 50 % (Fig. 6C). Two plant secondary metabolites that are also volatile aromatic aldehydes, cinnamaldehyde and vanillin, exhibited significant fluorescence inhibition. Cinnamaldehyde had an IC50 of 0.360 ± 0.002 mM and K_i of 0.337 mM, whereas vanillin demonstrated an IC50 value of 1.077 ± 0.020 mM and K_i of 1.009 mM. As for caffeic acid, a phenylpropanoid biosynthesis product, it had an IC50 value of 0.968 ± 0.049 mM and K_i of 0.906 mM. Additionally, chlorogenic acid, an ester of quinic acid and caffeic acid, exhibited an IC50 of 0.480 ± 0.013 mM and Ki of 0.450 mM. Lastly, the pesticide metabolites tested 2,4-dichlorophenol and TCPy gave IC50 values of 1.322 ± 0.022 mM and 1.119 ± 0.043 mM, and Ki values of 1.238 mM and 1.048 mM, respectively.

Table 1
Kinetic parameters for LdGSTs2.

Substrate	V_{max} (μM/min)	h	K_{half} (mM)	k_{cat} (min^{-1})	k_{cat}/K_{half} ($min^{-1} \cdot mM^{-1}$)
CDNB	1023.12 ± 73.64	1.54 ± 0.11	3.20 ± 0.34	263.73	82.41
GSH	197.07 ± 5.35	–	0.13 ± 0.02	50.80	390.77

3.6. Crystal structure and molecular docking analysis of LdGSTs2

LdGSTs2 crystallized in the space group $P2_1$ with unit cell dimensions a = 49.372 Å, b = 88.781 Å, c = 97.902 Å, and angles α = 90°, β = 99.73°, γ = 90°. There were four LdGSTs2 molecules in the asymmetric unit, composed of two dimers. The LdGSTs2 structure (PDB ID 9P6K) was refined to a resolution of 2.8 Å, with R-work at 0.2232 and R-free at 0.2738. Full crystal data statistics can be found in Table 3.

HHpred (https://toolkit.tuebingen.mpg.de/tools/hhpred) was used to search for sequence homologues to LdGSTs2 and to perform comparative analysis. The resulting structural sequence alignment is shown in Fig. S3. The closest homologue was a sigma GST from *Blattella germanica* (PDB ID 4Q5R), with a homologue probability score of 100 %, sequence identity at 40 % and similarity score at 0.796. GSTs2 (PDB ID 5H5L) from *N. lugens* also displayed the highest sequence identity at 44

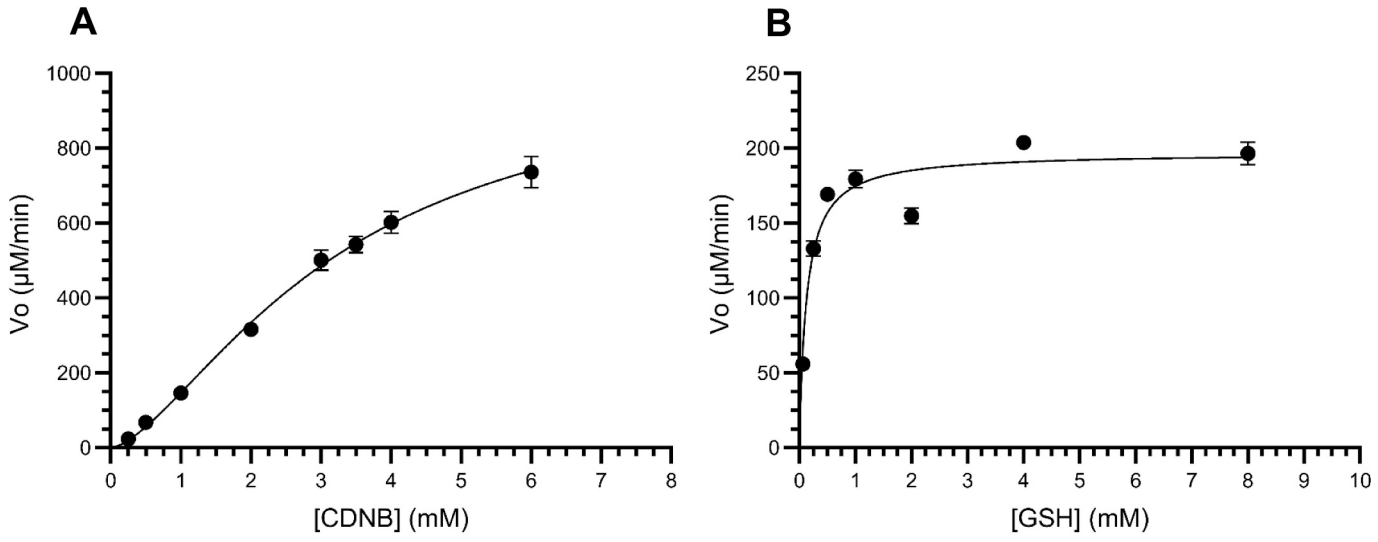

Fig. 4. The steady-state initial velocities of recombinant LdGSTs2 at varying substrate concentrations. Initial velocities were determined for both CDNB as the variable substrate and holding GSH fixed (A), and GSH as the variable substrate and CDNB fixed (B).

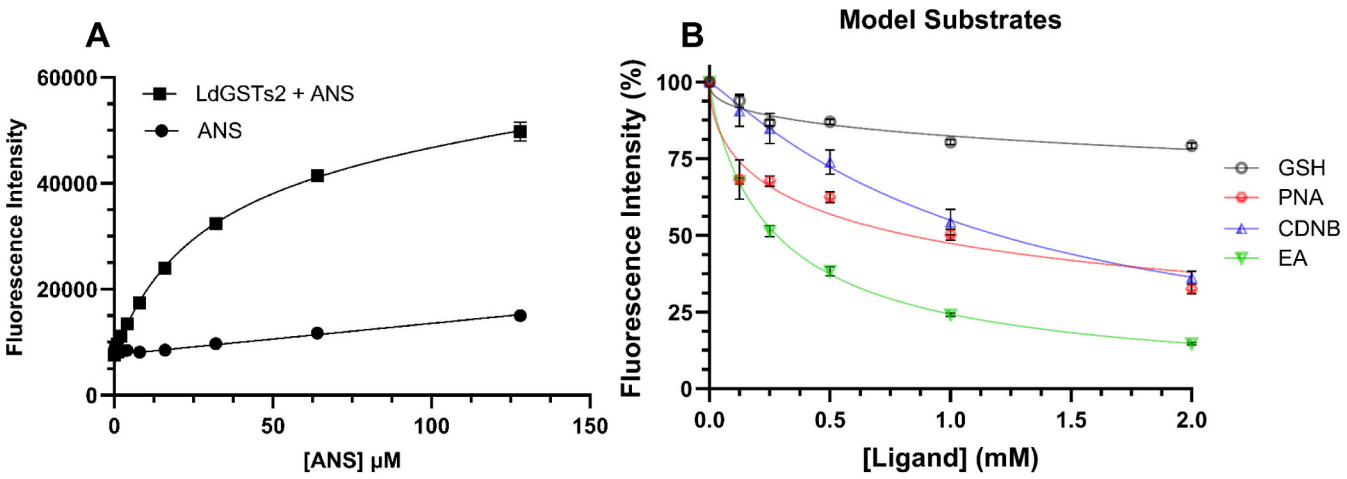

Fig. 5. Competitive binding curves of model substrate to purified recombinant LdGSTs2 protein. (A) Binding curve of LdGSTs2 with the fluorescent probe ANS and the fluorescence of ANS alone. Fluorescence intensity is plotted on the y-axis with ANS concertation on the x-axis. (B) LdGSTs2 binding curves with co-substrate GSH or model substrates PNA, CDNB, and EA. Fluorescence intensity is plotted on the y-axis with ligand/substrate concertation on the x-axis.

Table 2
Ligand binding data for LdGSTs2.

Category	Ligand	IC50 (mM)	Ki (mM)
Model ligands	GSH	–	–
	CDNB	1.199 ± 0.057	0.775
	Ethacrynic Acid	0.280 ± 0.005	1.123
	PNA	0.828 ± 0.093	0.262
Fungicide	Propiconazloe	–	–
Herbicides and metabolites	2,4-D	–	–
	2,4-Dichlorophenol	1.322 ± 0.022	1.238
	Dicamba	–	–
	Fenoprop	0.257 ± 0.003	0.241
	Picloram	–	–
	Triclopyr	1.572 ± 0.068	1.472
	2,4-Dichlorohenol	1.322 ± 0.022	1.238
Insecticides and metabolites	Acephate	–	–
	Acetamiprid	–	–
	Carbaryl	–	–
	Chlorpyrifos	0.166 ± 0.016	0.155
	Chlothianidin	–	–
	Imidacloprid	–	–
	Malathion	–	–
	Methamidophos	–	–
	TCPy	1.119 ± 0.043	1.048
	Thiamethoxam	–	–
Potato allelochemicals	Caffeic Acid	0.968 ± 0.049	0.906
	Chlorogenic Acid	0.480 ± 0.013	0.450
	Cinnamaldehyde	0.360 ± 0.002	0.337
	p-Coumaric Acid	–	–
	Vanillin	1.077 ± 0.020	1.009

% as compared to LdGSTs2 with a similarity score of 0.828, and homologue probability score of 99.97 % [62]. Additionally, a sigma class GST form *Bombyx mori* (PDB ID 3VUR, PDB for GSH complex is 3VPQ) was a 99.97 % probable homologue with a sequence identity of 35 % and the similarity score was 0.655 [74]. Similarly, the sigma GST2 from *D. melanogaster* (PDB ID 1M0U) showed a probability score of 99.95 %, identify of 40 %, and similarity score of 0.757 [75]. A more distantly related *Homo sapiens* GSTp1 (PDB ID 5J41) had a probability score of 99.95 %, identity of 25 %, and similarity score of 0.316 [76]. To further analyze sigma class GST binding sites, the *H. sapiens* sigma class GST, hGSTS1–1 (PDB ID 3EE2) was identified and selected for analysis, because it was complexed with both GSH and the inhibitor nocodazole, the hGSTS-1 homologue had a probability score of 99.96 %, identity of 31 % and similarity score of 0.613 [77]. The homologues were used for multiple sequence structure alignment with LdGSTs2 at default alignment settings using the Chimera v1.16 MatchMaker tool. The structure alignment RMSDs for LdGSTs2 with 4Q5R, 5H5L, 3VPQ, 1M0U, 5 J41, and 3EE2 across all pairs were 1.384 Å, 1.830 Å, 1.991 Å, 1.213 Å, 2.452 Å, 3.836 Å, and with RMSDs for pruned pairs of 1.085 Å, 1.151 Å, 1.168 Å, 1.026 Å, 1.110 Å, 0.912 Å, respectively.

The LdGSTs2 structure displayed the canonical GST fold, displaying the typical two-domain α/β fold of GSTs. The LdGSTs2 structure crystalized in dimeric form, displaying two-fold symmetry (Fig. 7A and B). Each monomer consisted of two domains, the N-terminal and C-terminal domains, sometimes referred to as the G-domain and H-domain, respectively, based on their respective roles in binding the GSH substrate or a hydrophobic substrate [78]. The N-terminal displays an alpha/beta fold with the β-strands β1, β2, β3, and β4 comprising a central β-sheet that is flanked by helices α2 on the outside of the N-terminal domain, with α1 and α3 on the internal side of the N-terminal domain. After α3, there is a linker coil that connects the N-terminal domain with C-terminal domain. The H-domain (C-terminal domain) is a helical bundle composed of helices α4 through α9, and as with other GSTs is key in determining the hydrophobic substrate specificity of LdGSTs2 [78]. The dimer is held together by key interactions at the dimer interface between α3 and α4 on monomer A with α4 and α3 of monomer B (Fig. 7A and C). There are eight key interactions stabilizing the dimer at the interface, including two hydrogen bonds and six salt bridges (Fig. 7C). There is a hydrogen bond at a distance of 2.21 Å between Gln64 HE22 (α3 chain A) and Asp98 OD2 (α4 chain B), and a second complementary hydrogen bond between Gln64 HE22 (α3 chain B) and Asp98 OD2 (α4 chain A) at distance of 2.48 Å (Fig. 7C). Additionally, there are the six salt bridges at the dimer interface; the first three being between the Lys75 NZ atom on α3 of chain A and the Glu83 OE2 atom of α4 on chain B at 3.26 Å distant, next there is a salt bridge between the Arg70 NH1 atom of α3 on chain A and Asp90 OD2 atom of α4 on chain B at a distance of 3.32 Å, and also between the Arg70 NH1 atom of α3 on chain A located at a distance of 3.28 Å from the Asp90 OD1 atom of α4 on chain B. Then, the other three complementary salt bridges between Lys75 NZ atom (α3 chain B) and Glu83 OE2 atom (α4 chain A) at 3.54 Å apart, Arg70 NH1 atom (α3 chain B) and Asp90 atom OD2 (α4 chain A) at 3.56 Å distant, and lastly, the Arg70 NH1 atom located 3.27 Å (α3 chain B) from the Asp90 OD1 atom (α4 chain A) (Fig. 7C).

There are two active sites within the LdGSTs2 dimer (Fig. 7D), with each monomer containing one active site. Additionally, the LdGSTs2 active site contains two binding sites: the G-site which binds GSH and the H-site which binds a hydrophobic substrate. In GSTs, the H-site has been shown to interact with both exogenous and endogenous electrophilic substrates [21,40,79]. Since LdGSTs2 crystallized in apo form, the active site was identified by structural comparison with homologues,

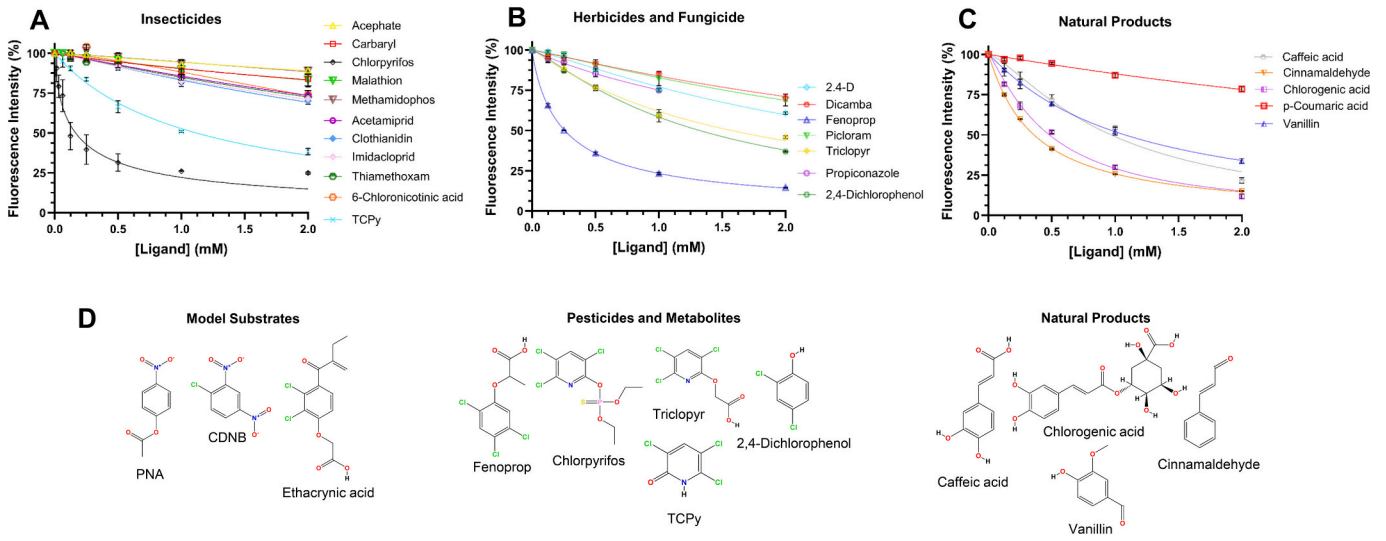

Fig. 6. Competitive binding curves for potential ligands of LdGSTs2 showing changes in fluorescence intensity as a function of increasing ligand concentrations. Fluorescence inhibition indicates displacement of ANS from H-site, resulting from ligand binding. (A) Insecticides and metabolites, (B) Fungicides, herbicides and metabolites, (C) Natural products from potato plants. (D) Chemical structures of the ligands that resulted in 50 % or greater decrease in fluorescence intensity are shown.

Table 3
Data collection and refinement of the LdGSTs2 crystal structure.

PDB ID	9P6K
Beamline	MacCHESS 7B2
Data collection	
Wavelength (Å)	0.9686
Resolution range	29.20–2.84 (2.88–2.84)
Space group	P1 21 1
Unit cell	49.37 88.78 97.90 90.00 99.73 90.00
Total reflections	70,459 (2339)
Unique reflections	20,483 (722)
Multiplicity	3.4 (3.2)
Completeness (%)	97.3 (95.65)
Mean I/sigma (I)	7.73 (1.16)
Wilson B-factor	76.2
R-merge	0.08801 (1.103)
R-meas	0.1044 (1.323)
R-pim	0.05569 (0.7198)
CC1/2	0.997 (0.432)
CC*	0.999 (0.777)
Refinement	
Reflections used for refinement	19,726 (780)
Reflections used for R-free	1932 (69)
R-work	0.2203 (0.4223)
R-free	0.2675 (0.4535)
Number of non-hydrogen atoms	6888
macromolecules	6888
ligands	0
solvent	0
Protein residues	840
RMS (bonds)	0.010
RMS (angles)	1.14
Ramachandran favored (%)	96.51
Ramachandran allowed (%)	3.49
Ramachandran outliers (%)	0.00
Rotamer outliers (%)	0.52
Clashscore	9.90
Average B-factor	106.08
Macromolecules	106.08

followed by molecular docking with GSH, chlorpyrifos and chlorogenic acid (Fig. 8). The highest scoring pose of GSH (−6.309 kcal/mol) docked in the G-site was consistent in location and atom positioning when LdGSTs2 was superimposed onto homologous crystal structures, that were complexed with GSH molecules. Based on the molecular docking study, the G-site residues of LdGSTs2 consisted of Tyr9, Phe10, Arg15, Phe40, Lys 44, Gln51, Leu52, Gln64, and Ser65 (Fig. 8A). Key binding interactions of GSH within the LdGSTs2 G-site included Tyr 9, with its hydroxyl within hydrogen bond distance of the GSH thiolate sulfur, located 3.0 Å apart. Additionally, a salt bridge was formed between the glycyl carboxylate of GSH located 3.2 Å from the Lys44 NZ atom. There was a hydrogen bond with the Gln51 HE22 hydrogen atom located 2.6 Å from the glycyl O2 carboxylate oxygen of GSH. Additionally, the backbone carbonyl of Leu52 formed a hydrogen bond with the glycyl amine at 3.1 Å. Another hydrogen bond formed between the Gln64 OE1 atom at 3.4 Å away from the glutamyl amine of GSH. Lastly, the Ser65 hydroxyl formed a hydrogen bond with the glutamyl carboxylate of GSH (3.2 Å).

The H-site is located adjacent to the G-Site and formed by a solvent exposed pocket running from Arg15 across to α4 and α6, then back to the coil connecting α8 and α9 of the C-terminal domain as pictured by the transparent pink surface (Fig. 8B). The residues making up the H-site pocket were identified as Asp11, Phe12, Thr13, Gly14, Arg15, Pro18, Lys100, Lys101, Ser104, Ala107, Tyr108, Cys159, Ala160, Glu162, Thr163, Asn166, Met167, Lys169, Asn202, Met204, Leu205, and Ser206. The volume of the H-site pocket was calculated to be 680 $Å^3$, sufficient to accommodate ligands larger than the model substrate CDNB and ligands such as chlorogenic acid or chlorpyrifos. Molecular docking showed that chlorogenic acid (Fig. 8C) and chlorpyrifos (Fig. 8D) bind to LdGSTs2 with docking scores of −6.439 kcal/mol and − 5.762 kcal/mol, respectively. These findings, in conjunction with fluorescence binding assay data, suggest that chlorogenic acid and chlorpyrifos may act as potential substrates.

4. Discussion

Arthropod GSTs confer xenobiotic adaptation through direct conjugation of chemicals or indirectly by providing protection against oxidative stress induced by xenobiotic exposure [25]. Previous synergism studies using GST inhibitors have demonstrated that GSTs contribute to insecticide resistance in numerous CPB populations [35–37]. In this study, we aimed to test whether a sigma class GST, *LdGSTs2,* upregulated in a resistant strain and inducible by potato leaf feeding, contributes to the species' robust capacities for both insecticide resistance and host plant adaptation. Combined techniques including molecular biology, functional genomics, enzyme kinetics and binding assay, as well as crystallography and molecular docking were used to

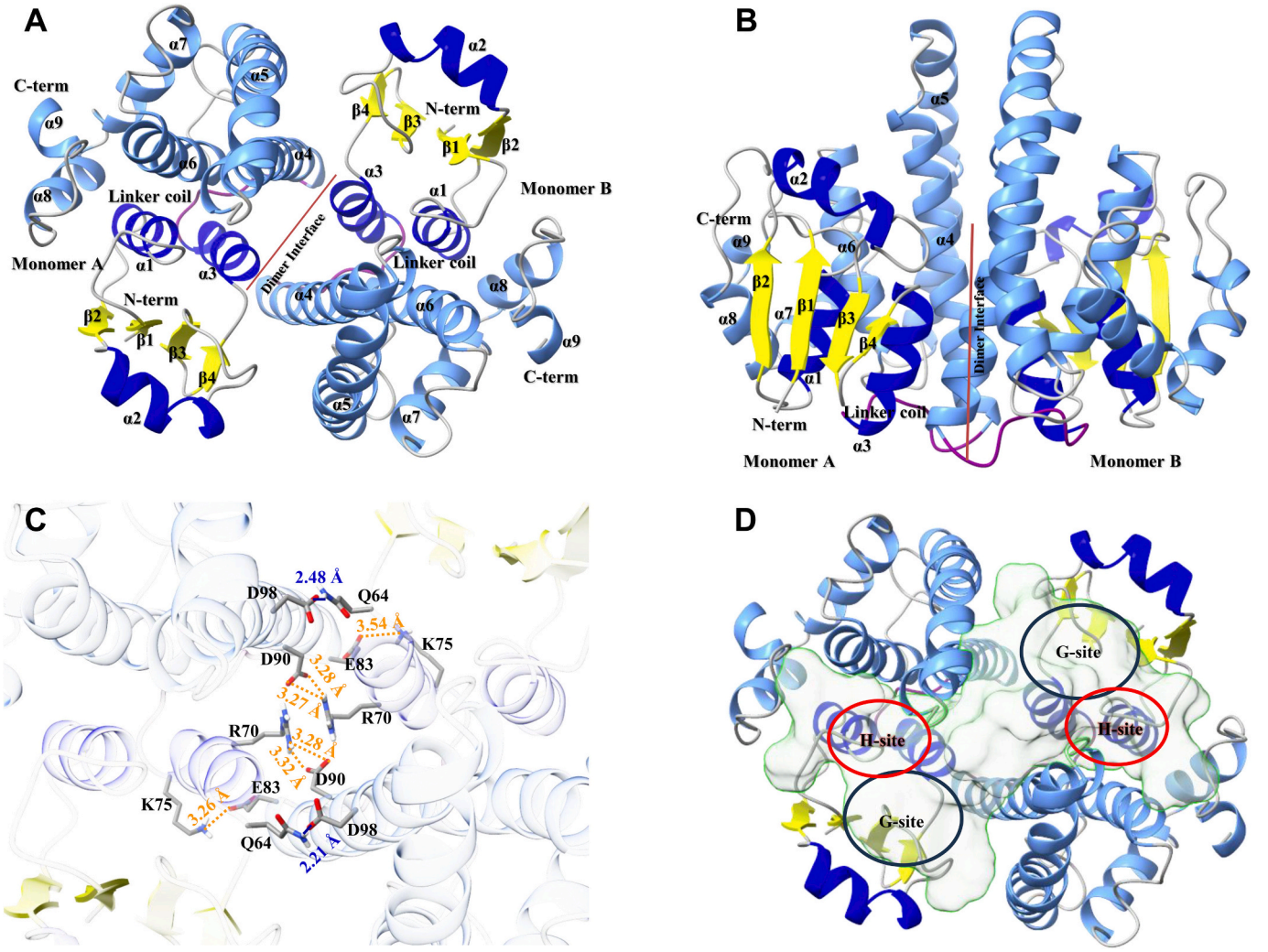

Fig. 7. LdGSTs2 protein crystal structure. (A) The global dimeric structure of LdGSTs2, showing monomer A and monomer B. The β-strands and helices are number from in order from the n-terminus to c-terminus. The N-terminal domain has helices colored dark blue and strands colored yellow. The C-terminal domain has helices colored light blue. The N-terminal domain is connected to the C-terminal domain by a peptide linkage "linker coil" colored purple. (B) LdGSTs2 structure oriented to emphasize the 2-fold symmetry and location of residues involved in the dimer interface interactions. (C) Zoomed in view of dimer interface interactions. Interaction distances are shown and given in angstroms, salt bridges are colored orange and hydrogen bonds in blue. (D) The H-site and G-site in both monomers are shown. The solvent accessible pocket in the dimmer composed of the two active sites connected by a solvent accessible channel is shown as a transparent surface representation. (For interpretation of the references to colour in this figure legend, the reader is referred to the web version of this article.)

test our hypothesis.

Gene expression analysis showed that *LdGSTs2* was overexpressed in the insecticide-resistant CPB strain compared to the susceptible one. Feeding on potato leaves induced up to 18-fold *LdGSTs2 expression* compared to that in CPBs fed on an artificial diet (Fig. 2). This strong induction by host plant material suggests that *LdGSTs2* may be involved in the detoxification of plant-derived allelochemicals, such as those commonly found in the Solanaceae species. Since many of these compounds are metabolized by the same detoxification enzymes involved in insecticide resistance (e.g., cytochrome P450s and GSTs) [18], our findings support the hypothesis that *LdGSTs2* may contribute to cross-resistance by facilitating the detoxification of both plant toxins and synthetic insecticides. The spatial expression pattern of *LdGSTs2* in both susceptible and resistant strain revealed dominant expression in the midgut and Malpighian tubules, with some expression detected in the fat body of resistant CPB (Fig. 2B). These findings suggest that *LdGSTs2* could be contributing to insecticide resistance in CPB given that the midguts, Malpighian tubules, and fat body are major metabolic detoxification organs in insects. For example, in *Cydia pomonella*, several GSTs were found to be highly expressed in the Malpighian tubules, midgut or fat body as compared to other tissues [80,81]. Notably, *CpGSTs2* is highly expressed in the fat body, whereas *CpGSTe3* is predominately expressed in the midgut. The CDNB conjugation activity of both CpGSTs2 and CpGSTe3 were inhibited by insecticide λ-cyhalothrin, and both enzymes showed metabolic capacity toward it, suggesting their potential role in λ-cyhalothrin detoxification [80,81]. In the diamond-back moth, *Plutella xylostella*, one of the sigma GSTs, *PxGSTs1*, was highly expressed in the midgut and fat body, reflecting its potential roles in development of resistance to multiple insecticides [82]. RNAi is a widely used approach to functionally validate candidate genes involved in insecticide resistance [25,82–85]. Therefore, with this tool, we assessed the role of *LdGSTs2* in insecticide resistance of the CPB. Our data showed that the knockdown of *LdGSTs2* in the resistant CPB resulting in enhanced susceptibility to imidacloprid, suggesting the likely involvement of *LdGSTs2* in insecticide resistance.

Enzymatic activity toward the common GST substrate CDNB, in the presence of the co-substrate GSH, generally suggests the catalytic function of a specific GST enzyme [26]. In our study, the *Km* values for CDNB and GSH were 3.20 ± 0.02 mM and 0.13 ± 0.02 mM, respectively (Fig. 4; Table 2). These are comparable to values reported in other insect

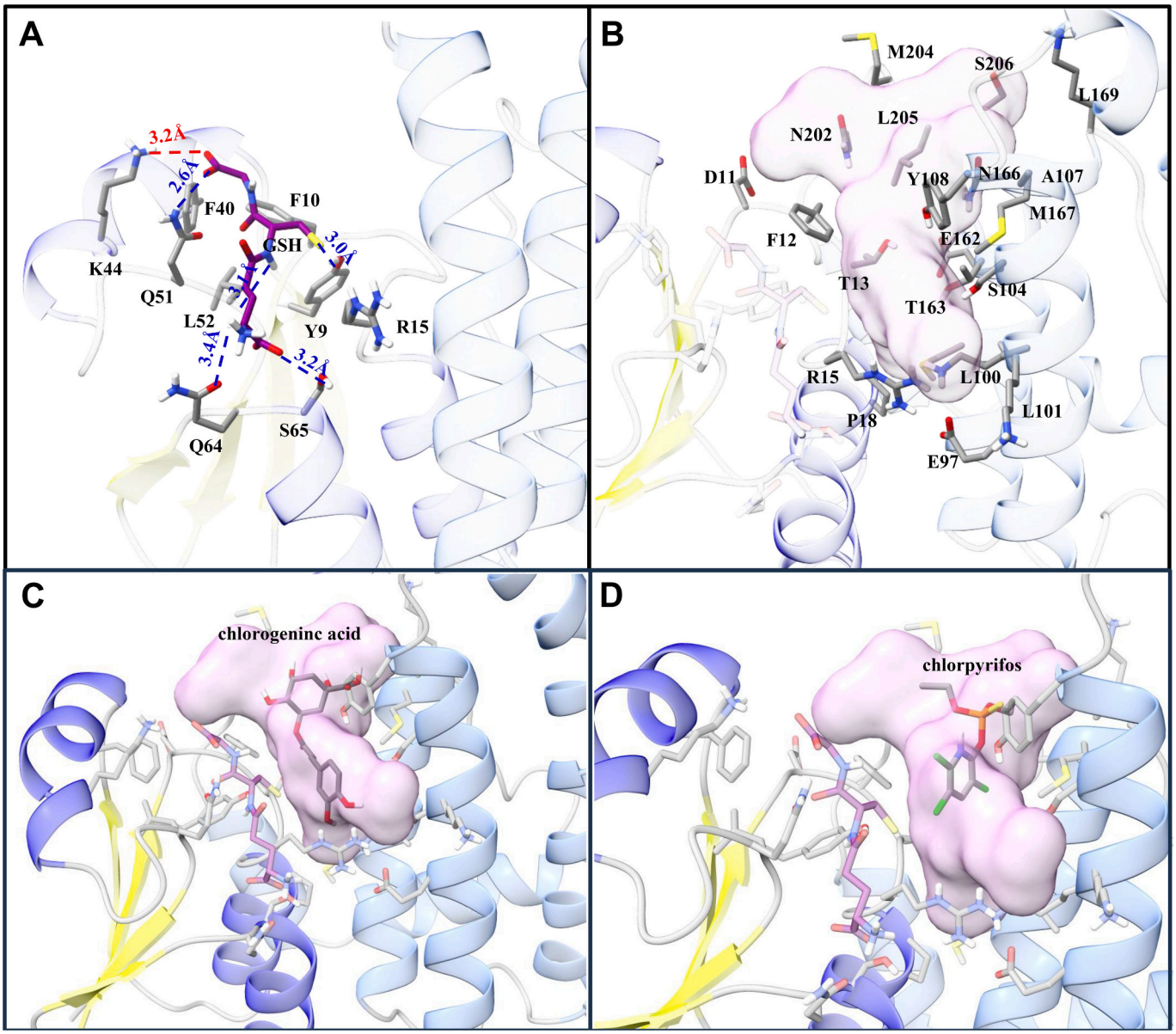

Fig. 8. LdGSTs2 active sites and molecular docking with xenobiotics. (A) The G-site with docked GSH. Hydrogen bonds are shown in blue and the salt bridge shown in red. (B) The binding pocket for the H-site is shown as pink transparent surface. Additionally, the sidechain residues making up the pocket are shown. (C) The G-site with chlorogenic acid docked. (D) The G-site with chlorpyrifos docked. (For interpretation of the references to colour in this figure legend, the reader is referred to the web version of this article.)

and mite GSTs [82,85–87], supporting its functional identity as a GST and suggesting conserved catalytic properties across GST classes. GSTs are known to function through two primary mechanisms: one involves catalytic conjugation of glutathione (GSH) to xenobiotic compounds, while the other involves non-catalytic sequestration, in which GSTs bind and sequester xenobiotics without enzymatic conjugation [25]. Both mechanisms depend on the enzyme's capacity to bind these compounds. To investigate the binding capacity, we performed competitive binding assays using ANS as a fluorescence reporter. These assays were designed to evaluate whether various pesticides and natural products could compete with ANS for binding to the purified recombinant LdGSTs2. We observed that LdGSTs2 exhibited a unique binding capacity with a variety of pesticides and potato-derived natural products. Among the chemicals screened, we found organophosphate insecticide chlorpyrifos and its primary metabolite TCPy, as well as herbicides fenoprop, triclopyr and 2,4-D metabolite 2,4-Dichlorophenol inhibited ANS by 50 % or more, suggesting strong binding affinity of these pesticides and their metabolites to LdGSTs2. In addition to synthetic pesticides, LdGSTs2 also showed binding affinity to several plant-derived natural products, including chlorogenic acid, p-coumaric acid, and caffeic acid. Exposure to plant secondary metabolites has been proposed as one factor contributing to the rapid evolution of insecticide resistance in insects and mites, potentially through the co-option of detoxification enzymes that act on both insecticides and plant allelochemicals [16–18,88]. Chlorogenic acid, a major phenolic compound in potato leaves, plays a key role in plant defense due to its antimicrobial properties, particularly against pathogens such as bacteria and fungi [9]. Its levels have been reported to increase following leaf damage, including herbivory by chewing insects, as part of the plant's inducible defense response [10–12]. Similarly, caffeic acid, a hydroxycinnamic acid and common phenolic allelochemical in potato leaves, also contributes to plant defense through its antioxidant and antimicrobial activities [14,15]. Recent evidence suggests that high concentrations of caffeic acid can negatively affect the development, growth, and physiological processes

in insects [14]. However, in adapted insect species such as the CPB, chronic exposure to phenolic compounds like chlorogenic and caffeic acid may induce detoxification and antioxidant defense pathways. Due to their antioxidant properties, these compounds may also help insects mitigate oxidative stress caused by pesticide exposure or pathogen infection. Our RNAi results suggest that LdGSTs2 may be involved in imidacloprid resistance. However, our binding assays did not show significant inhibition of ANS fluorescence by imidacloprid (Fig. 6A), indicating a lack of direct binding. In this case, we hypothesize that the role of *LdGSTs2* in insecticide resistance may be mediated through its function in mitigating oxidative stress rather than direct detoxification. Future studies will be needed to test this hypothesis.

Our crystal structure data suggested a possible Ligandin function with a dimer interface pocket that may serve to bind or sequester toxic compounds. In Fig. 7B, the LdGSTs2 dimer has been oriented showing the area where the key dimer interactions occur (span shown by red bar). As pictured in Fig. 7B and D, above the dimer interface interactions the protein is opened to solvent, forming a solvent exposed channel. The solvent exposed channel connects the active site in monomer A to the active site in monomer B (Fig. 7D). In a previous study by Ji et al., a sigma class GST from *Nototodarus sloanii* (PDB ID 2GSQ) was crystalized with the ligand S-(3-iodobenzyl) GSH complexed and bound in the solvent channel between active sites [89]. Additionally, a GST from *Schistosoma japonicum* (PDB ID 6RWD) was observed to bind a larger polyphenolic compound ellagic acid that formed a crystal complex with ellagic acid bound in the solvent channel [90]. Given previous examples from the sigma class, the solvent-accessible channel connecting active sites in the LdGSTs2 dimmer could serve as an auxiliary binding site for non-substrates ligands and potentially function in sequestration or transport.

To fully resolve the precise binding interactions, future research could integrate site-directed mutagenesis with kinetic assays to experimentally validate the roles of key residues, as demonstrated in previous studies [79,82,91]. In parallel, obtaining high-resolution co-crystal structures and conducting targeted metabolism assays will further refine our understanding of the binding interactions and catalytic determinants [92,93]. These complementary approaches would provide deeper insights into the molecular determinants of substrate specificity and catalytic activity.

5. Conclusions

Overall, we performed an integrative study revealing that the sigma-class GST *LdGSTs2* may play a dual role in detoxifying both insecticides and host plant-derived compounds in CPB. Functional evidence from RNAi experiments demonstrated its contribution to imidacloprid resistance, while biochemical and structural analyses supported its broad substrate-binding capacity. These findings provide direct evidence that host plant adaptation and insecticide resistance may share overlapping molecular mechanisms, mediated by multifunctional detoxification enzymes like GSTs. Our work underscores the evolutionary plasticity of pest species and highlights the importance of targeting such enzymes in the design of next-generation, sustainable pest management strategies.

Supplementary data to this article can be found online at https://doi.org/10.1016/j.ijbiomac.2025.147108.

CRediT authorship contribution statement

Timothy W. Moural: Writing – review & editing, Writing – original draft, Visualization, Validation, Software, Methodology, Investigation, Funding acquisition, Formal analysis, Data curation, Conceptualization. **Jonathan A. Hernandez:** Writing – original draft, Methodology, Investigation, Formal analysis. **Qi-Ren Chen:** Writing – original draft, Methodology, Investigation, Formal analysis. **B.K. Sonu Koirala:** Visualization, Software, Methodology. **Yanjun Liu:** Methodology, Formal analysis. **Tristan M. Cofer:** Software, Methodology. **Isadora X. Zuo:** Writing – review & editing, Investigation. **Andrei Alyokhin:** Writing – review & editing, Resources, Methodology. **Haichuan Wang:** Writing – review & editing, Software, Methodology, Formal analysis, Data curation. **Fang Zhu:** Writing – review & editing, Writing – original draft, Validation, Supervision, Resources, Project administration, Funding acquisition, Formal analysis, Data curation, Conceptualization.

Ethics approval

This article does not contain any studies with human or vertebrate animal subjects.

Funding

This work was supported by NSF CAREER IOS-2144082, the USDA National Institute of Food and Federal Appropriations under Hatch Project #PEN04770 and Accession #1010058 (to FZ). TM was supported by USDA NIFA postdoctoral fellowship, grant #2020-67034-31780/project accession #1022959 (2020-2022) and USDA NIFA Hatch Project #PEN04897 and Accession #7005652.

Declaration of competing interest

The authors declare that they have no known competing financial interests or personal relationships that could have appeared to influence the work reported in this paper.

Data availability

Data will be made available on request.

References

[1] D. Weber, Colorado beetle: pest on the move, Pestic. Outlook 14 (2003) 256–259.
[2] A. Alyokhin, M. Baker, D. Mota-Sanchez, G. Dively, E. Grafius, Colorado potato beetle resistance to insecticides, Am. J. Potato Res. 85 (6) (2008) 395–413.
[3] S. Mishra, J. Dee, W. Moar, J. Dufner-Beattie, J. Baum, N.P. Dias, A. Alyokhin, A. Buzza, S.I. Rondon, M. Clough, S. Menasha, R. Groves, J. Clements, K. Ostlie, G. Felton, T. Waters, W.E. Snyder, J.L. Jurat-Fuentes, Selection for high levels of resistance to double-stranded RNA (dsRNA) in Colorado potato beetle (*Leptinotarsa decemlineata* say) using non-transgenic foliar delivery, Sci. Rep. 11 (1) (2021) 6523.
[4] D. Mota-Sanchez, R.M. Hollingworth, E.J. Grafius, D.D. Moyer, Resistance and cross-resistance to neonicotinoid insecticides and spinosad in the Colorado potato beetle, *Leptinotarsa decemlineata* (say) (Coleoptera: Chrysomelidae), Pest Manag. Sci. 62 (1) (2006) 30–37.
[5] Y.H. Chen, Z.P. Cohen, E.M. Bueno, B.M. Christensen, S.D. Schoville, Rapid evolution of insecticide resistance in the Colorado potato beetle, *Leptinotarsa decemlineata*, Curr. Opin. Insect Sci. 55 (2023) 101000.
[6] A. Cingel, J. Savic, J. Lazarevic, T. Cosic, M. Raspor, A. Smigocki, S. Ninkovic, Extraordinary adaptive plasticity of Colorado potato beetle: "ten-striped spearman" in the era of biotechnological warfare, Int. J. Mol. Sci. 17 (9) (2016).
[7] C. Rodríguez-Pérez, A.M. Gómez-Caravaca, E. Guerra-Hernández, L. Cerretani, B. García-Villanova, V. Verardo, Comprehensive metabolite profiling of *Solanum tuberosum* L. (potato) leaves by HPLC-ESI-QTOF-MS, Food Res. Int. 112 (2018) 390–399.
[8] P.A. Divekar, S. Narayana, B.A. Divekar, R. Kumar, B.G. Gadratagi, A. Ray, A. K. Singh, V. Rani, V. Singh, A.K. Singh, A. Kumar, R.P. Singh, R.S. Meena, T. K. Behera, Plant secondary metabolites as defense tools against herbivores for sustainable crop protection, Int. J. Mol. Sci. 23 (5) (2022).
[9] H. Akyol, Y. Riciputi, E. Capanoglu, M.F. Caboni, V. Verardo, Phenolic compounds in the potato and its byproducts: an overview, Int. J. Mol. Sci. 17 (6) (2016).
[10] G.W. Felton, K.K. Donato, R.M. Broadway, S.S. Duffey, Impact of oxidized plant phenolics on the nutritional quality of dietar protein to a noctuid herbivore, *Spodoptera exigua*, J. Insect Physiol. 38 (4) (1992) 277–285.
[11] A. Bhonwong, M.J. Stout, J. Attajarusit, P. Tantasawat, Defensive role of tomato polyphenol oxidases against cotton bollworm (*Helicoverpa armigera*) and beet armyworm (*Spodoptera exigua*), J. Chem. Ecol. 35 (1) (2009) 28–38.
[12] Y. Liao, L. Zeng, S. Rao, D. Gu, X. Liu, Y. Wang, H. Zhu, X. Hou, Z. Yang, Induced biosynthesis of chlorogenic acid in sweetpotato leaves confers the resistance against sweetpotato weevil attack, J. Adv. Res. 24 (2020) 513–522.
[13] P. Kumar, E.V. Ortiz, E. Garrido, K. Poveda, G. Jander, Potato tuber herbivory increases resistance to aboveground lepidopteran herbivores, Oecologia 182 (1) (2016) 177–187.

[14] A. Punia, V. Singh, A. Thakur, N.S. Chauhan, Impact of caffeic acid on growth, development and biochemical physiology of insect pest, *Spodoptera litura* (Fabricius), Heliyon 9 (3) (2023) e14593.
[15] A.R. War, M.G. Paulraj, B. Hussain, A.A. Buhroo, S. Ignacimuthu, H.C. Sharma, Effect of plant secondary metabolites on legume pod borer, *Helicoverpa armigera*, J. Pest. Sci. 86 (3) (2013) 399–408.
[16] F. Zhu, T.W. Moural, D.R. Nelson, S.R. Palli, A specialist herbivore pest adaptation to xenobiotics through up-regulation of multiple cytochrome P450s, Sci. Rep. 6 (2016) 20421.
[17] A. Alyokhin, Y.H. Chen, Adaptation to toxic hosts as a factor in the evolution of insecticide resistance, Curr. Opin. Insect Sci. 21 (2017) 33–38.
[18] L. Despres, J.P. David, C. Gallet, The evolutionary ecology of insect resistance to plant chemicals, Trends Ecol. Evol. 22 (6) (2007) 298–307.
[19] W. Dermauw, N. Wybouw, S. Rombauts, B. Menten, J. Vontas, M. Grbić, R. M. Clark, R. Feyereisen, T. Van Leeuwen, A link between host plant adaptation and pesticide resistance in the polyphagous spider mite (*Tetranychus urtica*), Proc. Natl. Acad. Sci. U. S. A. 110 (2) (2013) E113–E122.
[20] C. Cruse, T.W. Moural, F. Zhu, Dynamic roles of insect carboxyl/cholinesterases in chemical adaptation, Insects 14 (2) (2023) 194.
[21] B.K.S. Koirala, T. Moural, F. Zhu, Functional and structural diversity of insect glutathione S-transferases in xenobiotic adaptation, Int. J. Biol. Sci. 18 (15) (2022) 5713–5723.
[22] A. Pym, K.S. Singh, Å. Nordgren, T.G.E. Davies, C.T. Zimmer, J. Elias, R. Slater, C. Bass, Host plant adaptation in the polyphagous whitefly, *Trialeurodes vaporariorum*, is associated with transcriptional plasticity and altered sensitivity to insecticides, BMC Genomics 20 (1) (2019) 996.
[23] B. Pélissié, Y.H. Chen, Z.P. Cohen, M.S. Crossley, D.J. Hawthorne, V. Izzo, S. D. Schoville, Genome resequencing reveals rapid, repeated evolution in the Colorado potato beetle, Mol. Bio. Evol. 39 (2) (2022).
[24] A.A. Enayati, H. Ranson, J. Hemingway, Insect glutathione transferases and insecticide resistance, Insect Mol. Biol. 14 (1) (2005) 3–8.
[25] N. Pavlidi, J. Vontas, T. Van Leeuwen, The role of glutathione S-transferases (GSTs) in insecticide resistance in crop pests and disease vectors, Curr. Opin. Insect Sci. 27 (2018) 97–102.
[26] W.H. Habig, M.J. Pabst, W.B. Jakoby, Glutathione S-transferases. The first enzymatic step in mercapturic acid formation, J. Biol. Chem. 249 (22) (1974) 7130–7139.
[27] G.W. Felton, C.B. Summers, Antioxidant systems in insects, Arch. Insect Biochem. Physiol. 29 (2) (1995) 187–197.
[28] Y. Liu, F. Zhu, Z. Shen, T.W. Moural, L. Liu, Z. Li, X. Liu, H. Xu, Glutaredoxins and thioredoxin peroxidase involved in defense of emamectin benzoate induced oxidative stress in *Grapholita molesta*, Pestic. Biochem. Physiol. 176 (2021) 104881.
[29] C. Frova, Glutathione transferases in the genomics era: new insights and perspectives, Biomol. Eng. 23 (4) (2006) 149–169.
[30] C. He, W. Xie, X. Yang, S.L. Wang, Q.J. Wu, Y.J. Zhang, Identification of glutathione S-transferases in Bemisia tabaci (Hemiptera: Aleyrodidae) and evidence that GSTd7 helps explain the difference in insecticide susceptibility between B. tabaci Middle East-minor Asia 1 and Mediterranean, Insect Mol. Biol. 27 (1) (2018) 22–35.
[31] A.J. Ketterman, C. Saisawang, J. Wongsantichon, Insect glutathione transferases, Drug Metab. Rev. 43 (2) (2011) 253–265.
[32] S.-s. Gao, D.-y. Li, Z.-k. Huo, Y.-l. Zhang, Y.-z. Cao, Y.-y. Tan, X.-l. Guo, J.-h. Zhang, K.-p. Zhang, R.-m. Li, A sigma class glutathione S-transferase gene regulated by the CncC pathway is required for phytochemical tolerance in the red flour beetle, *Tribolium castaneum*, J. Asia Pac. Entomol. 25 (4) (2022) 102004.
[33] J.U. Flanagan, M.L. Smythe, Sigma-class glutathione transferases, Drug Metab. Rev. 43 (2) (2011) 194–214.
[34] Y. Zhang, B. Yang, N. Yu, G. Luo, H. Gao, X. Lin, Z. Liu, Insecticide resistance associated overexpression of two sigma GST genes assists *Nilaparvata lugens* to remedy oxidative stress from feeding on resistant rice variety, Pestic. Biochem. Physiol. 188 (2022) 105230.
[35] M. Malek Mohamadi, M.S. Mossadegh, M.J. Hejazi, M.T. Goodarzi, M. Khanjani, H. Galehdari, Synergism of resistance to phosalone and comparison of kinetic properties of acetylcholinesterase from four field populations and a susceptible strain of Colorado potato beetle, Pestic. Biochem. Physiol. 98 (2) (2010) 254–262.
[36] W.H. Jiang, Z.T. Wang, M.H. Xiong, W.P. Lu, P. Liu, W.C. Guo, G.Q. Li, Insecticide resistance status of Colorado potato beetle (Coleoptera: Chrysomelidae) adults in northern Xinjiang Uygur autonomous region, J. Econ. Entomol. 103 (4) (2010) 1365–1371.
[37] W.-H. Jiang, W.-C. Guo, W.-P. Lu, X.-Q. Shi, M.-H. Xiong, Z.-T. Wang, G.-Q. Li, Target site insensitivity mutations in the AChE and *LdVssc1* confer resistance to pyrethroids and carbamates in *Leptinotarsa decemlineata* in northern Xinjiang Uygur autonomous region, Pestic. Biochem. Physiol. 100 (1) (2011) 74–81.
[38] J. Clements, S. Schoville, N. Peterson, A.S. Huseth, Q. Lan, R.L. Groves, RNA interference of three up-regulated transcripts associated with insecticide resistance in an imidacloprid resistant population of *Leptinotarsa decemlineata*, Pestic. Biochem. Physiol. 135 (2017) 35–40.
[39] S.D. Schoville, Y.H. Chen, M.N. Andersson, J.B. Benoit, A. Bhandari, J.H. Bowsher, et al., A model species for agricultural pest genomics: the genome of the Colorado potato beetle, *Leptinotarsa decemlineata* (Coleoptera: Chrysomelidae), Sci. Rep. 8 (1) (2018) 1931.
[40] Y. Liu, T. Moural, S. Koirala B K, J. Hernandez, Z. Shen, A. Alyokhin, F. Zhu, Structural and functional characterization of one unclassified glutathione S-transferase in xenobiotic adaptation of Leptinotarsa decemlineata, Int. J. Mol. Sci. 22 (21) (2021) 11921.
[41] J.B. Han, G.Q. Li, P.J. Wan, T.T. Zhu, Q.W. Meng, Identification of glutathione S-transferase genes in *Leptinotarsa decemlineata* and their expression patterns under stress of three insecticides, Pestic. Biochem. Physiol. 133 (2016) 26–34.
[42] J. Chen, A. Alyokhin, D. Mota-Sanchez, M. Baker, M. Whalon, Variation in fitness among geographically isolated Colorado potato beetle (Coleoptera: Chrysomelidae) populations, Ann. Entomol. Soc. Am. 107 (1) (2014) 128–135.
[43] R.C. Edgar, MUSCLE: multiple sequence alignment with high accuracy and high throughput, Nucleic Acids Res. 32 (5) (2004) 1792–1797.
[44] K. Tamura, G. Stecher, S. Kumar, MEGA11: molecular evolutionary genetics analysis version 11, MBE 38 (7) (2021) 3022–3027.
[45] A. Stamatakis, RAxML-VI-HPC: maximum likelihood-based phylogenetic analyses with thousands of taxa and mixed models, Bioinformatics 22 (21) (2006) 2688–2690.
[46] T.W. Moural, L. Ban, J.A. Hernandez, M. Wu, C. Zhao, S.R. Palli, A. Alyokhin, F. Zhu, Silencing NADPH-cytochrome P450 reductase affects imidacloprid susceptibility, fecundity, and embryonic development in *Leptinotarsa decemlineata*, bioRxiv (2020), 2020.09.29.318634 1-19.
[47] K.J. Livak, T.D. Schmittgen, Analysis of relative gene expression data using real-time quantitative PCR and the 2(-delta delta C(T)) method, Methods (San Diego, Calif.) 25 (4) (2001) 402–408.
[48] F. Zhu, J. Xu, R. Palli, J. Ferguson, S.R. Palli, Ingested RNA interference for managing the populations of the Colorado potato beetle, *Leptinotarsa decemlineata*, Pest Manag. Sci. 67 (2) (2011) 175–182.
[49] D. Mota-Sanchez, R.M. Hollingworth, E.J. Grafius, D.D. Moyer, Resistance and cross-resistance to neonicotinoid insecticides and spinosad in the Colorado potato beetle, *Leptinotarsa decemlineata* (say) (Coleoptera: Chrysomelidae), Pest Manag. Sci. 62 (1) (2006) 30–37.
[50] J.Z. Zhao, B.A. Bishop, E.J. Grafius, Inheritance and synergism of resistance to imidacloprid in the Colorado potato beetle (Coleoptera: Chrysomelidae), J. Econ. Entomol. 93 (5) (2000) 1508–1514.
[51] J.A. Abendroth, T.W. Moural, C. Cruse, J.A. Hernandez, M. Wolfin, T.C. Baker, A. Alyokhin, F. Zhu, Pleiotropic functions of an antenna-specific odorant binding protein linking xenobiotic adaptation and olfaction in the Colorado potato beetle, *Leptinotarsa decemlineata*, bioRxiv (2025), 2025.04.29.651160 1-27.
[52] C.D. Kane, D.A. Bernlohr, A simple assay for intracellular lipid-binding proteins using displacement of 1-Anilinonaphthalene 8-sulfonic acid, Anal. Biochem. 233 (2) (1996) 197–204.
[53] Z. Yassin, E. Ortiz-Salmerón, F. García-Maroto, C. Barón, L. García-Fuentes, Implications of the ligandin binding site on the binding of non-substrate ligands to Schistosoma japonicum-glutathione transferase, Biochimica et Biophysica Acta (BBA) 1698 (2) (2004) 227–237.
[54] N. Kinsley, Y. Sayed, S. Mosebi, R.N. Armstrong, H.W. Dirr, Characterization of the binding of 8-anilinonaphthalene sulfonate to rat class Mu GST M1-1, Biophys. Chem. 137 (2) (2008) 100–104.
[55] H.J. Motulsky, R.R. Neubig, Analyzing binding data, Curr. Protoc. Neurosci. 52 (1) (2010) 7.5.1–7.5.65.
[56] GraphPad, Fitting binding of fluorescent ligands. https://www.graphpad.com/support/faq/fitting-binding-of-fluorescent-ligands/, 2024 (accessed 10 May 2024).
[57] C. D'Onofrio, V. Zaremska, J. Zhu, W. Knoll, P. Pelosi, Chapter ten - ligand-binding assays with OBPs and CSPs, in: P. Pelosi, W. Knoll (Eds.), Methods in Enzymology, Academic Press, Massachusetts, 2020, pp. 229–258.
[58] W. Kabsch, XDS, Acta Crystallogr. D. 66 (2) (2010) 125–132.
[59] A.J. McCoy, R.W. Grosse-Kunstleve, P.D. Adams, M.D. Winn, L.C. Storoni, R. J. Read, Phaser crystallographic software, J. Appl. Cryst. 40 (4) (2007) 658–674.
[60] D. Liebschner, P.V. Afonine, M.L. Baker, G. Bunkoczi, V.B. Chen, T.I. Croll, et al., Macromolecular structure determination using X-rays, neutrons and electrons: recent developments in Phenix, Acta Crystallogr. D. 75 (10) (2019) 861–877.
[61] P. Emsley, B. Lohkamp, W.G. Scott, K. Cowtan, Features and development of coot, Acta Crystallogr. D. 66 (4) (2010) 486–501.
[62] K. Yamamoto, A. Higashiura, M. Suzuki, K. Aritake, Y. Urade, A. Nakagawa, Molecular structure of a prostaglandin D synthase requiring glutathione from the brown planthopper, *Nilaparvata lugens*, Biochem. Biophys. Res. Commun. 492 (2) (2017) 166–171.
[63] J. Jumper, R. Evans, A. Pritzel, T. Green, M. Figurnov, O. Ronneberger, et al., Highly accurate protein structure prediction with AlphaFold, Nature 596 (7873) (2021) 583–589.
[64] M. Mirdita, K. Schütze, Y. Moriwaki, L. Heo, S. Ovchinnikov, M. Steinegger, ColabFold: making protein folding accessible to all, Nat. Methods 19 (6) (2022) 679–682.
[65] J. Agirre, M. Atanasova, H. Bagdonas, C.B. Ballard, A. Basle, J. Beilsten-Edmands, et al., The CCP4 suite: integrative software for macromolecular crystallography, Acta Crystallogr. D. 79 (6) (2023) 449–461.
[66] P.R. Evans, G.N. Murshudov, How good are my data and what is the resolution? Acta Crystallogr. D. 69 (7) (2013) 1204–1214.
[67] T.C. Terwilliger, R.W. Grosse-Kunstleve, P.V. Afonine, N.W. Moriarty, P.H. Zwart, L.-W. Hung, R.J. Read, P.D. Adams, Iterative model building, structure refinement and density modification with the PHENIX AutoBuild wizard, Acta Crystallogr. D. 64 (1) (2008) 61–69.
[68] P.V. Afonine, N.W. Moriarty, M. Mustyakimov, O.V. Sobolev, T.C. Terwilliger, D. Turk, A. Urzhumtsev, P.D. Adams, FEM: feature-enhanced map, Acta Crystallogr. D Biol. Crystallogr. 71 (Pt 3) (2015) 646–666.
[69] E.F. Pettersen, T.D. Goddard, C.C. Huang, G.S. Couch, D.M. Greenblatt, E.C. Meng, T.E. Ferrin, UCSF chimera—a visualization system for exploratory research and analysis, J. Comput. Chem. 25 (13) (2004) 1605–1612.

[70] E.C. Meng, T.D. Goddard, E.F. Pettersen, G.S. Couch, Z.J. Pearson, J.H. Morris, T. E. Ferrin, UCSF ChimeraX: Tools for structure building and analysis, Protein Sci. 32 (11) (2023) e4792.
[71] J. Eberhardt, D. Santos-Martins, A.F. Tillack, S. Forli, AutoDock Vina 1.2.0: new docking methods, expanded force field, and python bindings, J. Chem. Inf. Model. 61 (8) (2021) 3891–3898.
[72] E. Krissinel, K. Henrick, Inference of macromolecular assemblies from crystalline state, J. Mol. Biol. 372 (3) (2007) 774–797.
[73] C. Yung-Chi, W.H. Prusoff, Relationship between the inhibition constant (KI) and the concentration of inhibitor which causes 50 per cent inhibition (I50) of an enzymatic reaction, Biochem. Pharmacol. 22 (23) (1973) 3099–3108.
[74] K. Yamamoto, A. Higashiura, M. Suzuki, K. Aritake, Y. Urade, N. Uodome, A. Nakagawa, Crystal structure of a Bombyx mori sigma-class glutathione transferase exhibiting prostaglandin E synthase activity, Biochimica et Biophysica Acta (BBA) 1830 (6) (2013) 3711–3718.
[75] B. Agianian, P.A. Tucker, A. Schouten, K. Leonard, B. Bullard, P. Gros, Structure of a Drosophila sigma class glutathione S-transferase reveals a novel active site topography suited for lipid peroxidation products, J. Mol. Biol. 326 (1) (2003) 151–165.
[76] W. Harshbarger, S. Gondi, S.B. Ficarro, J. Hunter, D. Udayakumar, D. Gurbani, W. D. Singer, Y. Liu, L. Li, J.A. Marto, K.D. Westover, Structural and biochemical analyses reveal the mechanism of glutathione- S-Transferase Pi 1 inhibition by the anti-cancer compound piperlongumine*, J. Biol. Chem. 292 (1) (2017) 112–120.
[77] J.E. Weber, A.J. Oakley, A.N. Christ, A.G. Clark, J.D. Hayes, R. Hall, D.A. Hume, P. G. Board, M.L. Smythe, J.U. Flanagan, Identification and characterisation of new inhibitors for the human hematopoietic prostaglandin D2 synthase, Eur. J. Med. Chem. 45 (2) (2010) 447–454.
[78] B. Wu, D. Dong, Human cytosolic glutathione transferases: structure, function, and drug discovery, Trends Pharmacol. Sci. 33 (12) (2012) 656–668.
[79] T.W. Moural, S. Koirala, B K, G. Bhattarai, Z. He, H. Guo, N.T. Phan, E.G. Rajotte, D.J. Biddinger, K. Hoover, F. Zhu, Architecture and potential roles of a delta-class glutathione S-transferase in protecting honey bee from agrochemicals, Chemosphere 350 (2024) 141089.
[80] C. Hu, W. Wang, D. Ju, G.M. Chen, X.L. Tan, D. Mota-Sanchez, X.Q. Yang, Functional characterization of a novel lambda-cyhalothrin metabolizing glutathione S-transferase, CpGSTe3, from the codling moth *Cydia pomonella*, Pest Manag. Sci. 76 (3) (2020) 1039–1047.
[81] C. Hu, Z. Wei, P. Li, J.D. Harwood, X. Li, X. Yang, Identification and funcitonal characterization of a sigma glutathione S-transferase CpGSTs2 involved in λ-cyhalothrin resistance in the codling moth Cydia pomonella, J. Agric. Food Chem. 68 (45) (2020) 12585–12594.
[82] J. Liu, Z. Tian, R. Li, S. Ni, H. Sun, F. Yin, Z. Li, Y. Zhang, Y. Li, Key contributions of the overexpressed *Plutella xylostella* sigma glutathione S-transferase 1 gene (*PxGSTs1*) in the resistance evolution to multiple insecticides, J. Agric. Food Chem. 72 (5) (2024) 2560–2572.
[83] F. Zhu, R. Parthasarathy, H. Bai, K. Woithe, M. Kaussmann, R. Nauen, D. A. Harrison, S.R. Palli, A brain-specific cytochrome P450 responsible for the majority of deltamethrin resistance in the QTC279 strain of *Tribolium castaneum*, Proc. Natl. Acad. Sci. U. S. A. 107 (19) (2010) 8557–8562.
[84] F. Zhu, Y. Cui, D.B. Walsh, L.C. Lavine, Application of RNAi towards insecticide resistance management, in: R. Chandrasekar, B.K. Tyagi, Z. Gui, G.R. Reeck (Eds.), Short Views on Insect Biochemistry and Molecular Biology, Academic Publisher, Manhattan, USA, 2014, pp. 595–619.
[85] X. Ma, J. Zeng, C. Zhang, W. Dai, Characterization of two glutathione S-transferase genes involved in clothianidin resistance in *Bradysia odoriphaga*, Pest Manag. Sci. 81 (3) (2025) 1360–1372.
[86] K. Yamamoto, N. Yamada, Identification of a diazinon-metabolizing glutathione S-transferase in the silkworm, Bombyx mori, Sci. Rep. 6 (1) (2016) 30073.
[87] N. Pavlidi, V. Tseliou, M. Riga, R. Nauen, T. Van Leeuwen, N.E. Labrou, J. Vontas, Functional characterization of glutathione S-transferases associated with insecticide resistance in *Tetranychus urticae*, Pestic. Biochem. Physiol. 121 (2015) 53–60.
[88] M.A. Morales, B.M. Mendoza, L.C. Lavine, M.D. Lavine, D.B. Walsh, F. Zhu, Selection of reference genes for expression studies of xenobiotic adaptation in *Tetranychus urticae*, Int. J. Biol. Sci. 12 (9) (2016) 1129–1139.
[89] X. Ji, E.C. von Rosenvinge, W.W. Johnson, R.N. Armstrong, G.L. Gilliland, Location of a potential transport binding site in a sigma class glutathione transferase by x-ray crystallography, Proc. Natl. Acad. Sci. U. S. A. 93 (16) (1996) 8208–8213.
[90] B.O. Akumadu, R. Pandian, J. Olfsen, R. Worth, M. Thulo, T. Mentor, S. Fanucchi, Y. Sayed, H.W. Dirr, I. Achilonu, Molecular basis of inhibition of *Schistosoma japonicum* glutathione transferase by ellagic acid: insights into biophysical and structural studies, Mol. Biochem. Parasitol. 240 (2020) 111319.
[91] Y. Li, R. Li, H. Shao, Z. Liu, X. Gao, Z. Tian, Y. Zhang, J. Liu, Unraveling key amino acid residues crucial for PxGSTs1 conferring benzoylurea insecticide resistance in *Plutella xylostella*, J. Agric. Food Chem. 72 (46) (2024) 25549–25559.
[92] C. Hu, J. Liu, W. Wang, D. Mota-Sanchez, S. He, Y. Shi, X. Yang, Glutathione S-transferase genes are involved in lambda-cyhalothrin resistance in *Cydia pomonella* via sequestration, J. Agric. Food Chem. 70 (7) (2022) 2256–2279.
[93] A.M. Hassell, G. An, R.K. Bledsoe, J.M. Bynum, H.L. Carter III, S.J. Deng, R. T. Gampe, T.E. Grisard, K.P. Madauss, R.T. Nolte, W.J. Rocque, L. Wang, K. L. Weaver, S.P. Williams, G.B. Wisely, R. Xu, L.M. Shewchuk, Crystallization of protein–ligand complexes, Acta Crystallogr. D Biol. Crystallogr. 63 (Pt 1) (2006) 72–79.